AD-A102 481 TERRA TEK INC SALT LAKE CITY UT F/G 19/4
SIMULATION OF THE LOAD-UNLOAD PATHS EXPERIENCED BY ROCK IN THE --ETC(U)
DEC 77 D R SCHMITZ, J N JOHNSON, R K DROPEK DNA001-76-C-0294
UNCLASSIFIED TR-76-74 DNA-4841F NL

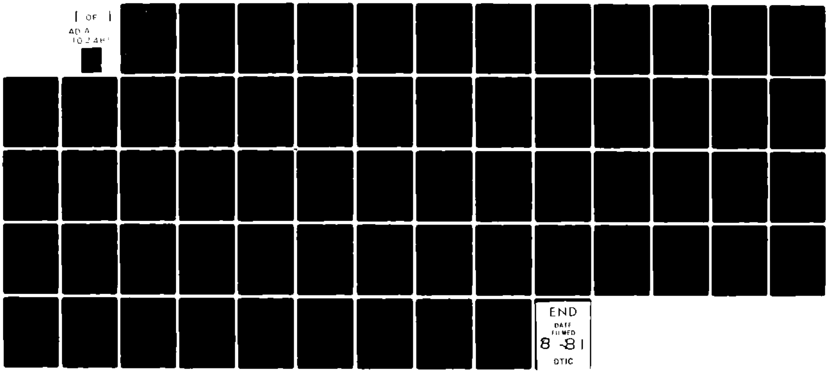

LEVEL II (10)

DNA 4841F

SIMULATION OF THE LOAD—UNLOAD PATHS EXPERIENCED BY ROCK IN THE VICINITY OF BURIED EXPLOSIONS

J. N. Johnson
R. K. Dropek
D. R. Schmitz
Terra Tek, Incorporated
420 Wakara Way
Salt Lake City, Utah 84108

1 December 1977

Final Report for Period 1 May 1976–1 December 1977

CONTRACT No. DNA 001-76-C-0294

APPROVED FOR PUBLIC RELEASE; DISTRIBUTION UNLIMITED.

THIS WORK SPONSORED BY THE DEFENSE NUCLEAR AGENCY UNDER RDT&E RMSS CODE B344076464 Y99QAXSB04903 H2590D.

Prepared for
Director
DEFENSE NUCLEAR AGENCY
Washington, D. C. 20305

Destroy this report when it is no longer needed. Do not return to sender.

PLEASE NOTIFY THE DEFENSE NUCLEAR AGENCY, ATTN: STTI, WASHINGTON, D.C. 20305, IF YOUR ADDRESS IS INCORRECT, IF YOU WISH TO BE DELETED FROM THE DISTRIBUTION LIST, OR IF THE ADDRESSEE IS NO LONGER EMPLOYED BY YOUR ORGANIZATION.

UNCLASSIFIED

SECURITY CLASSIFICATION OF THIS PAGE (When Data Entered)

REPORT DOCUMENTATION PAGE

READ INSTRUCTIONS BEFORE COMPLETING FORM

1. REPORT NUMBER DNA 4841F	2. GOVT ACCESSION NO. AD-A102 482	3. RECIPIENT'S CATALOG NUMBER
4. TITLE (and Subtitle) SIMULATION OF THE LOAD-UNLOAD PATHS EXPERIENCED BY ROCK IN THE VICINITY OF BURIED EXPLOSIONS		5. TYPE OF REPORT & PERIOD COVERED Final Report for Period 1 May 76 — 1 Dec 77
		6. PERFORMING ORG. REPORT NUMBER TR-76-74
7. AUTHOR(s) D. R. Schmitz J. N. Johnson R. K. Dropek		8. CONTRACT OR GRANT NUMBER(s) DNA 001-76-C-0294
9. PERFORMING ORGANIZATION NAME AND ADDRESS Terra Tek, Inc. 420 Wakara Way Salt Lake City, UT 84108		10. PROGRAM ELEMENT, PROJECT, TASK AREA & WORK UNIT NUMBERS Subtask Y99QAXSB049-03
11. CONTROLLING OFFICE NAME AND ADDRESS Director Defense Nuclear Agency Washington, D.C. 20305		12. REPORT DATE 1 December 1977
		13. NUMBER OF PAGES 62
14. MONITORING AGENCY NAME & ADDRESS (if different from Controlling Office)		15. SECURITY CLASS. (of this report) UNCLASSIFIED
		15a. DECLASSIFICATION/DOWNGRADING SCHEDULE N/A

16. DISTRIBUTION STATEMENT (of this Report)

Approved for public release; distribution unlimited

17. DISTRIBUTION STATEMENT (of the abstract entered in Block 20, if different from Report)

18. SUPPLEMENTARY NOTES

This work sponsored by the Defense Nuclear Agency under RDT&E RMSS Code B344076464 Y99QAXSB04903 H2590D.

19. KEY WORDS (Continue on reverse side if necessary and identify by block number)

Kayenta Sandstone
Strain and Stress Paths Buried Explosions
Finite Difference Solutions

20. ABSTRACT (Continue on reverse side if necessary and identify by block number)

Theoretical and experimental results are presented which define the strain paths and stress paths experienced by geological material elements in the vicinity of buried explosions. The theoretical strain and stress paths are obtained by finite-difference solution of spherical and cylindrical explosions in an infinite inelastic medium. These calculations are used to define loading and unloading paths in static laboratory tests on Kayenta sandstone. The data presented here thus provide the necessary information for definition of material contitutive models which apply to these specific explosive geometries.

UNCLASSIFIED

SECURITY CLASSIFICATION OF THIS PAGE(*When Data Entered*)

UNCLASSIFIED

SECURITY CLASSIFICATION OF THIS PAGE(*When Data Entered*)

TABLE OF CONTENTS

LIST OF ILLUSTRATIONS

LIST OF ILLUSTRATIONS (Cont)

LIST OF ILLUSTRATIONS (Cont)

LIST OF TABLES

INTRODUCTION

Common testing procedures for the laboratory measurement of material properties for use in ground motion calculations have generally consisted of standard hydrostatic, uniaxial-strain and triaxial tests. It has recently been recognized that these paths are not necessarily the ones that are followed in actual field applications, i.e., conventional and nuclear explosions in the earth. Since difficulty is often experienced in developing accurate constitutive models that are valid for a wide range of loading conditions, it seems important to follow, as closely as possible, the stress paths (or strain paths) that are experienced by material elements in actual field conditions. Furthermore, since measurement techniques do not yet allow the field determination of these stress paths (or strain paths), one must rely on numerical calculations and an initial best estimation of the material constitutive properties. In this report we present the results of one-dimensional numerical finite-difference calculations for cylindrical and spherical wave propagation, which define the stress and strain paths followed by material elements at varying distances from cylindrical and spherical explosive sources in the earth. The purpose of these calculations is to define laboratory tests best suited for the definition of material constitutive behavior in the analysis of CIST (Cylindrical In Situ Tests) and other subsurface explosive events. On the basis of these calculational results, static laboratory tests are conducted which represent strain paths experienced by material elements in the vicinity of cylindrical and spherical explosions in an infinite medium. The material tested in the experimental program is Kayenta sandstone.

STRESS PATH DETERMINATION FROM FINITE-DIFFERENCE SOLUTIONS

The quantities which are obtained from the finite-difference solution are σ_i and ε_i as functions of time at various distances from the explosive source. For purposes of definite laboratory tests, it is useful to express the output of these calculations in terms of the load $L = \sigma_a - p_c$ and p_c in the triaxial test configuration. Here σ_a is the axial stress and p_c is the confining fluid pressure. It is also more convenient to deal with axial and transverse strain components (ε_a and ε_t) in the triaxial test rather than ε_i defined in the finite-difference solution. In the case of spherical flow, one would simply make the identification that $L = \sigma_1 - \sigma_3$, $p_c = \sigma_3$, $\varepsilon_a = \varepsilon_1$, and $\varepsilon_t = \varepsilon_3$. For cylindrical flow the identification is slightly more complicated.

In general, let us assume that we have values of stress and strain invariants defined by

$$\tau(t) \equiv [(\sigma_1-\sigma_2)^2 + (\sigma_2-\sigma_3)^2 + (\sigma_3-\sigma_1)^2]^{1/2}/\sqrt{6} \quad , \tag{1}$$

$$p(t) \equiv (\sigma_1 + \sigma_2 + \sigma_2)/3 \quad , \tag{2}$$

$$\varepsilon_v(t) \equiv \varepsilon_1 + \varepsilon_2 + \varepsilon_3 \quad , \tag{3}$$

$$\varepsilon_d(t) \equiv [(\varepsilon_1-\varepsilon_2)^2 + (\varepsilon_2-\varepsilon_3)^2 + (\varepsilon_3-\varepsilon_1)^2]^{1/2}/\sqrt{6} \quad , \tag{4}$$

as functions of time at a fixed spatial position as provided by the finite-difference calculation. If the material constitutive behavior involves only first and second invariants of the stress and strain tensors, the quantities defined by Eqs. (1) - (4) can also be written in the following terms for the purpose of defining laboratory test paths:

$$\tau(t) = (\sigma_a - p_c)/\sqrt{3} \quad , \tag{5}$$

$$p(t) = (\sigma_a + 2p_c)/3 \quad , \tag{6}$$

$$\varepsilon_v(t) = \varepsilon_a + 2\varepsilon_t \quad , \tag{7}$$

$$\varepsilon_d(t) = (\varepsilon_a - \varepsilon_t)/\sqrt{3} \quad , \tag{8}$$

and hence laboratory stress and strain paths become in parametric form (t as the parameter):

$$L = \sqrt{3}\,\tau(t) \quad , \tag{9}$$

$$p_c = p(t) - \tau(t)/\sqrt{3} \quad , \tag{10}$$

$$\varepsilon_a = \varepsilon_v(t)/3 + 2\varepsilon_d(t)/\sqrt{3} \quad , \tag{11}$$

$$\varepsilon_t = \varepsilon_v(t)/3 - \varepsilon_d(t)/\sqrt{3} \quad . \tag{12}$$

Calculational Results

Stress (and strain) paths for cylindrical and spherical wave propagation have been calculated with the use of elastic-plastic constitutive descriptions presented in the Appendix. The material parameters are chosen to be representative of Mixed Company (Kayenta) sandstone. In all cases a radial stress given by

$$\sigma_r = p_o e^{-\alpha t} \tag{13}$$

is applied at the interior cavity surface of radius $R_o = 1$ m. The peak radial stress, p_o, is taken to be 10 kbar and the decay constant, $1/\alpha$, takes on values of 0.1 msec, 1.0 msec and 10 msec. All results are presented in terms of ε_a vs. ε_t (axial strain vs. transverse strain) and L/μ vs. p_c/K (load/shear-modulus vs. confining-fluid-pressure/bulk-modulus), i.e., the quantities related directly to static triaxial laboratory tests.

Figures 1a, 1b and 1c show stress and strain paths at various distances from a cylindrical explosion. At the radial position $R = 2R_o$ the stress path intersects the failure surface during loading and remains in contact during unloading. The corresponding strain path initially approximates conditions of uniaxial strain, but exhibits considerable transverse strain during the latter stages of deformation. At $R = 3R_o$ it can be seen that the strain path is approximated by loading in uniaxial strain followed by unloading at constant axial strain, while at $R = 5R_o$ the axial strain is seen to decrease during unloading. Of course, at much greater distances from the explosive source plane-wave conditions are achieved, and the load-unload path remains on the $\varepsilon_t = 0$ axis.

Figures 2a - 2e show similar behavior for spherical wave propagation. Figures 1 and 2 give an indication of how strain and stress paths depend on distance from the source. Another important consideration is that of pulse shape or pulse duration. This is controlled by the parameter α in Eq. (13). A number of calculations were performed for cylindrical geometry with $1/\alpha$ = 0.1 msec, 1.0 msec and 10 msec. The peak radial stress p_o remains the same in all calculations (p_o = 10 kbar). The resulting stress and strain paths are shown in Figure 3 at radial positions $1.5R_o$, $2R_o$, $3R_o$, $4R_o$ and $5R_o$. One sees immediately that not only does the position have influence on stress and strain paths, but also that pulse duration has a significant effect. It will therefore be important to represent, as accurately as possible, the time history of the cavity stress due to the explosive source.

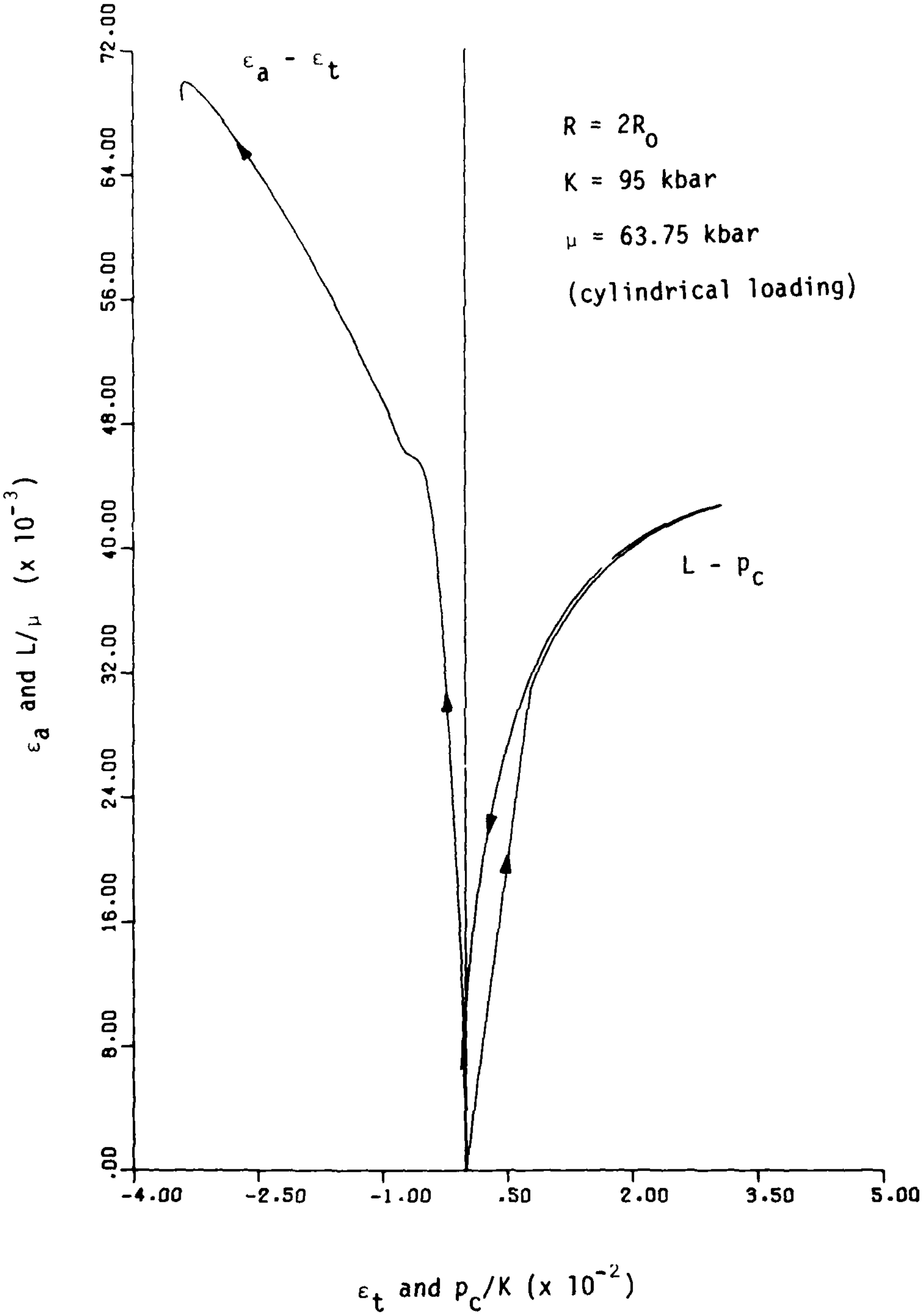

Figure 1a. Strain paths and stress paths at $R = 2R_o$ cylindrical wave propagation in Mixed Company sandstone. A radial stress given by $\sigma_r = p_o \exp(-\alpha t)$, with $(1/\alpha) = 1$ msec and $p_o = 10$ kbar, is applied at $R_o = 1$ m.

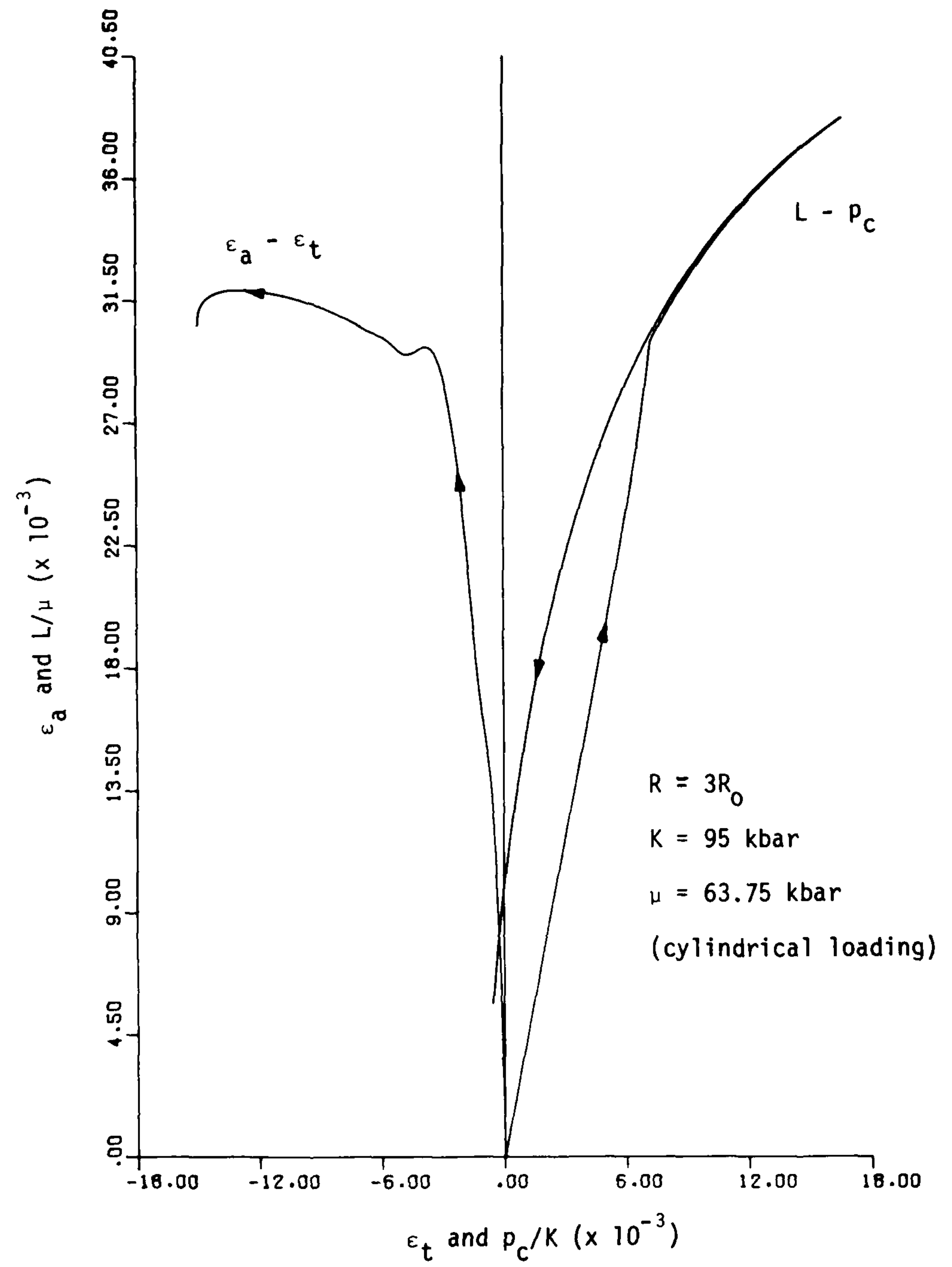

Figure 1b. Same as 1a, but with $R = 3R_o$. Note changes in vertical and horizontal scales.

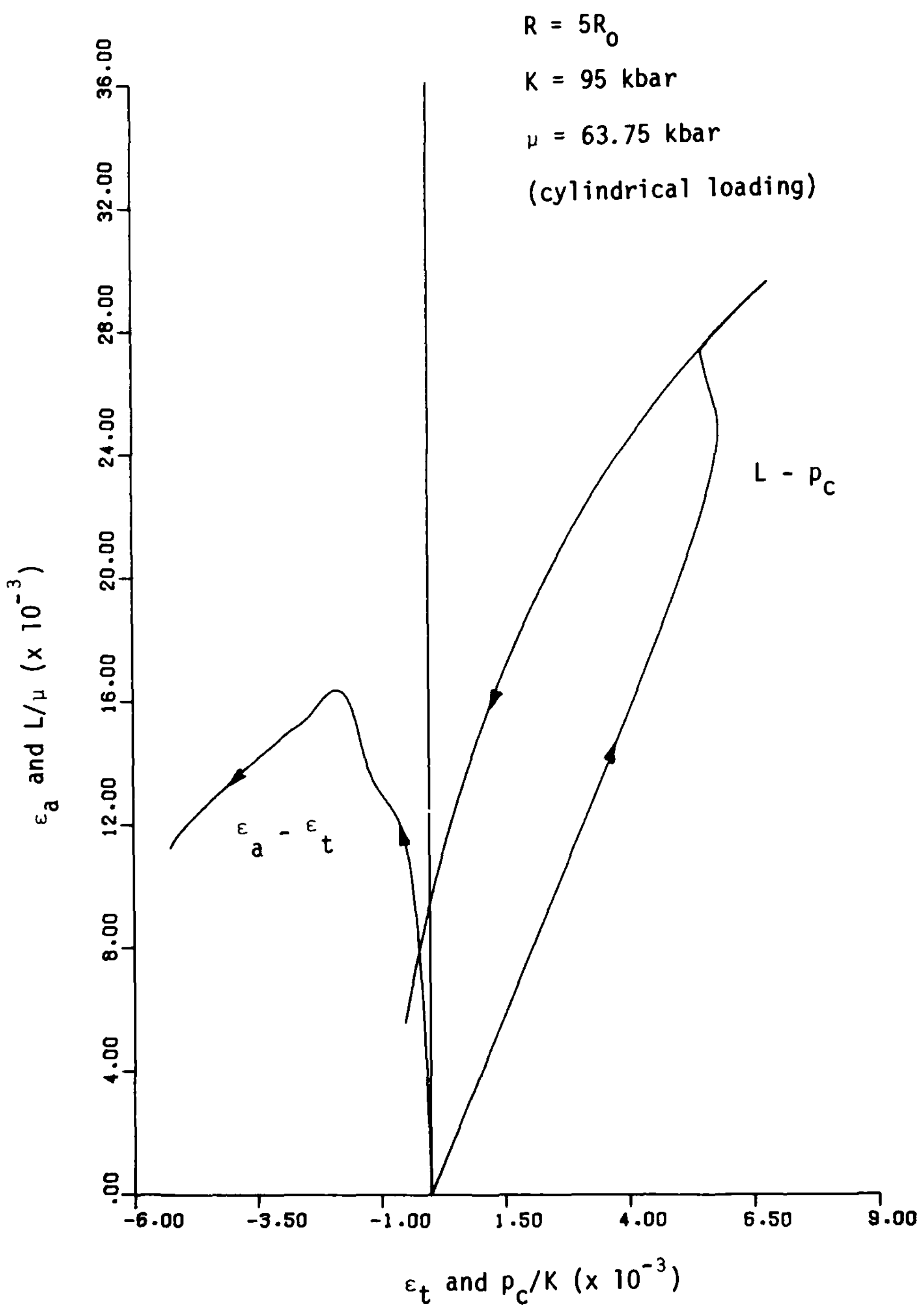

Figure 1c. Same as 1a, but with $R = 5R_0$. Note changes in vertical and horizontal scales.

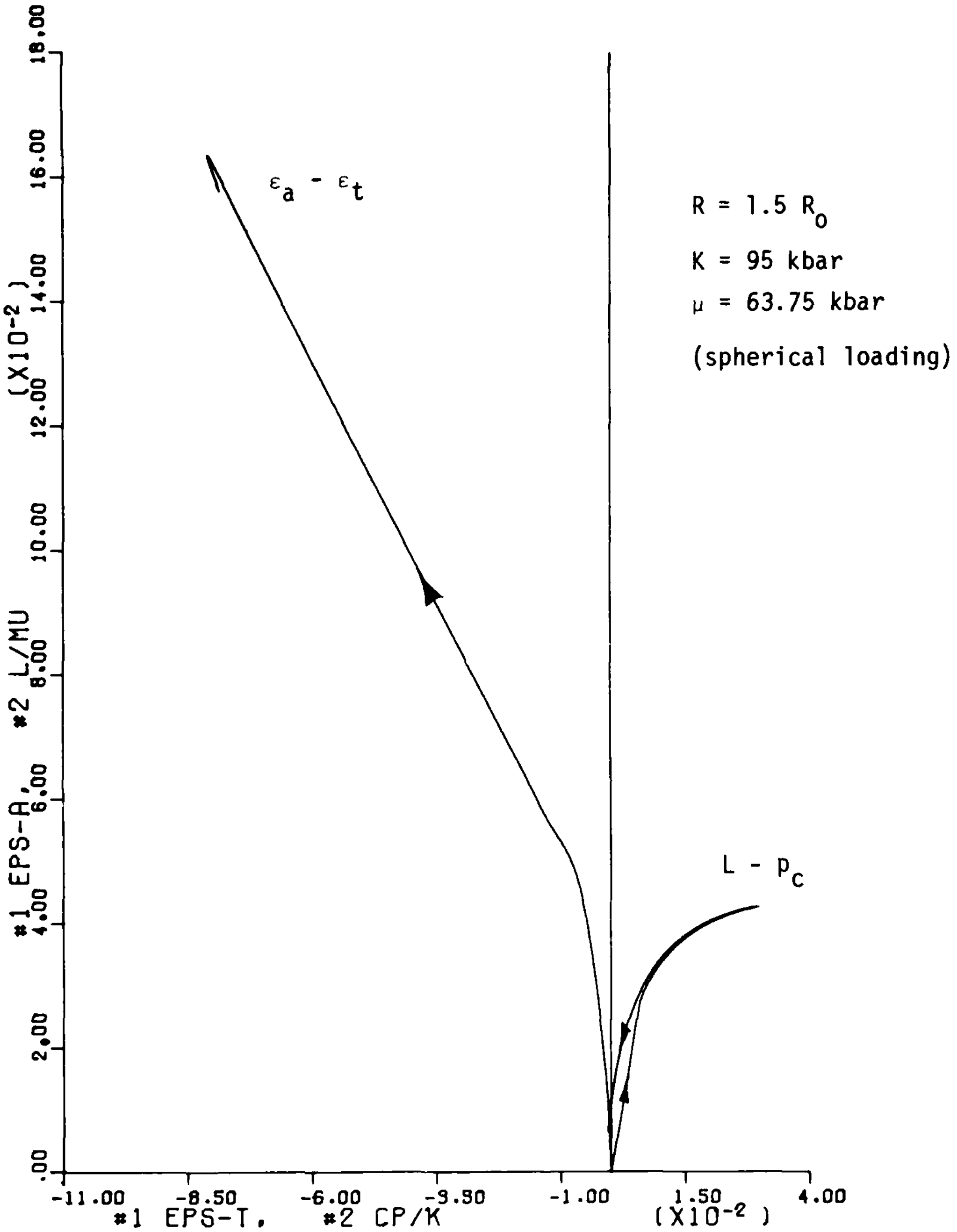

Figure 2a. Strain paths and stress paths at R = 1.5R_0 for spherical wave propagation in Mixed Company sandstone. A radial stress given by $\sigma_r = p_o \exp(-\alpha t)$, with $1/\alpha$ = 1 msec and p_o = 10 kbar, is applied at R_o = 1 m.

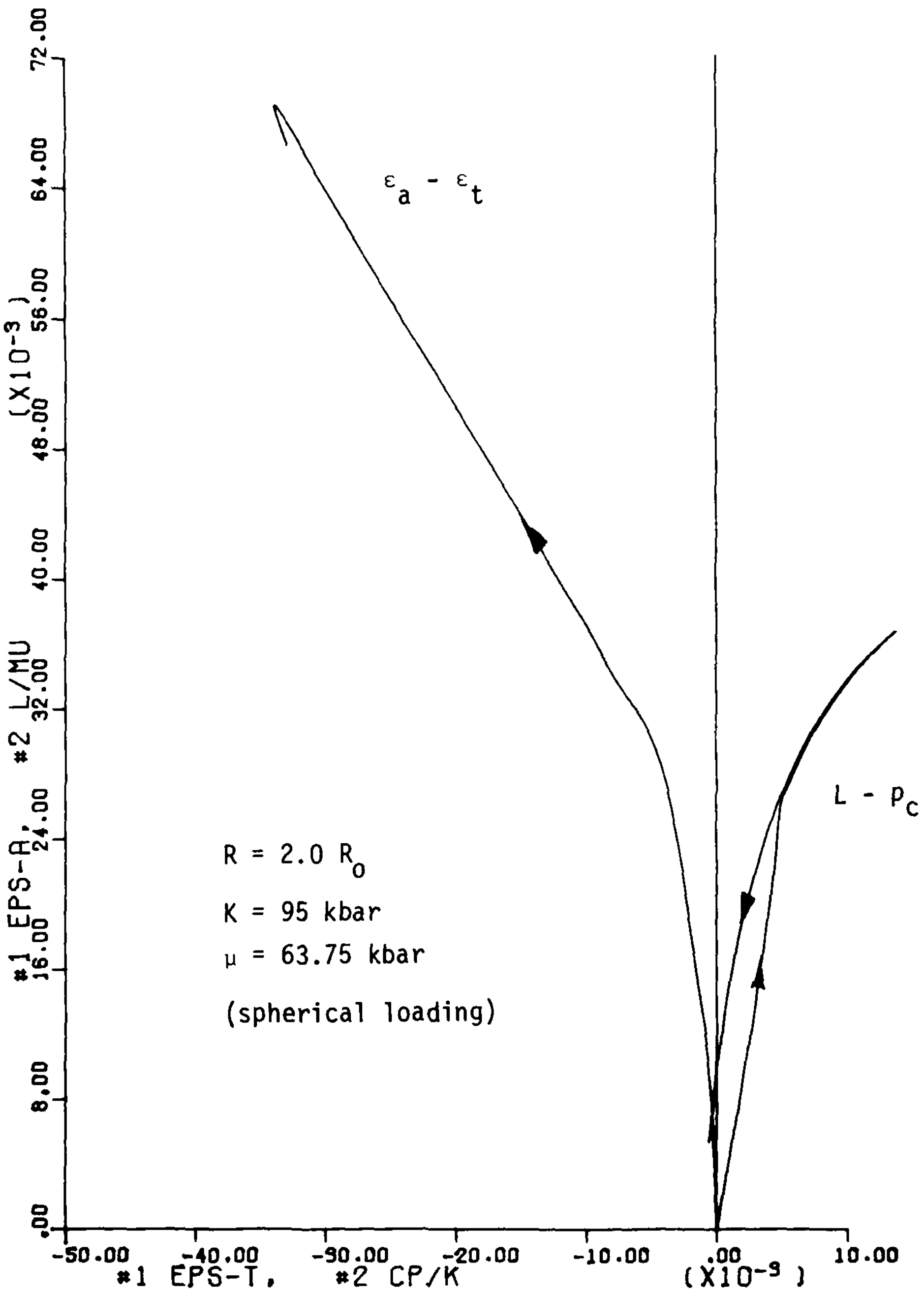

Figure 2b. Same as 2a, but with $R = 2R_0$. Note changes in vertical and horizontal scales.

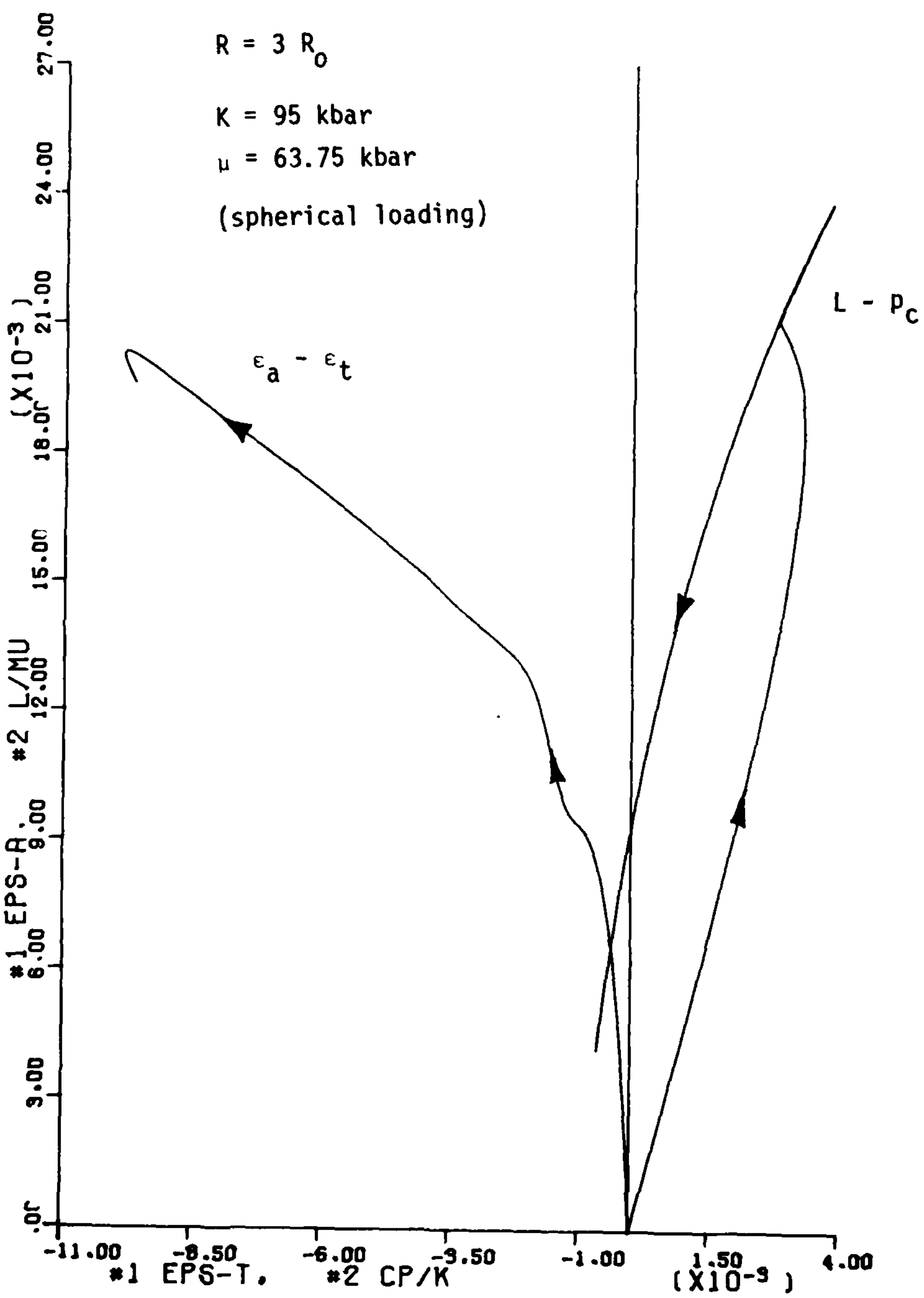

Figure 2c. Same as 2a, but with $R = 3R_o$. Note changes in vertical and horizontal scales.

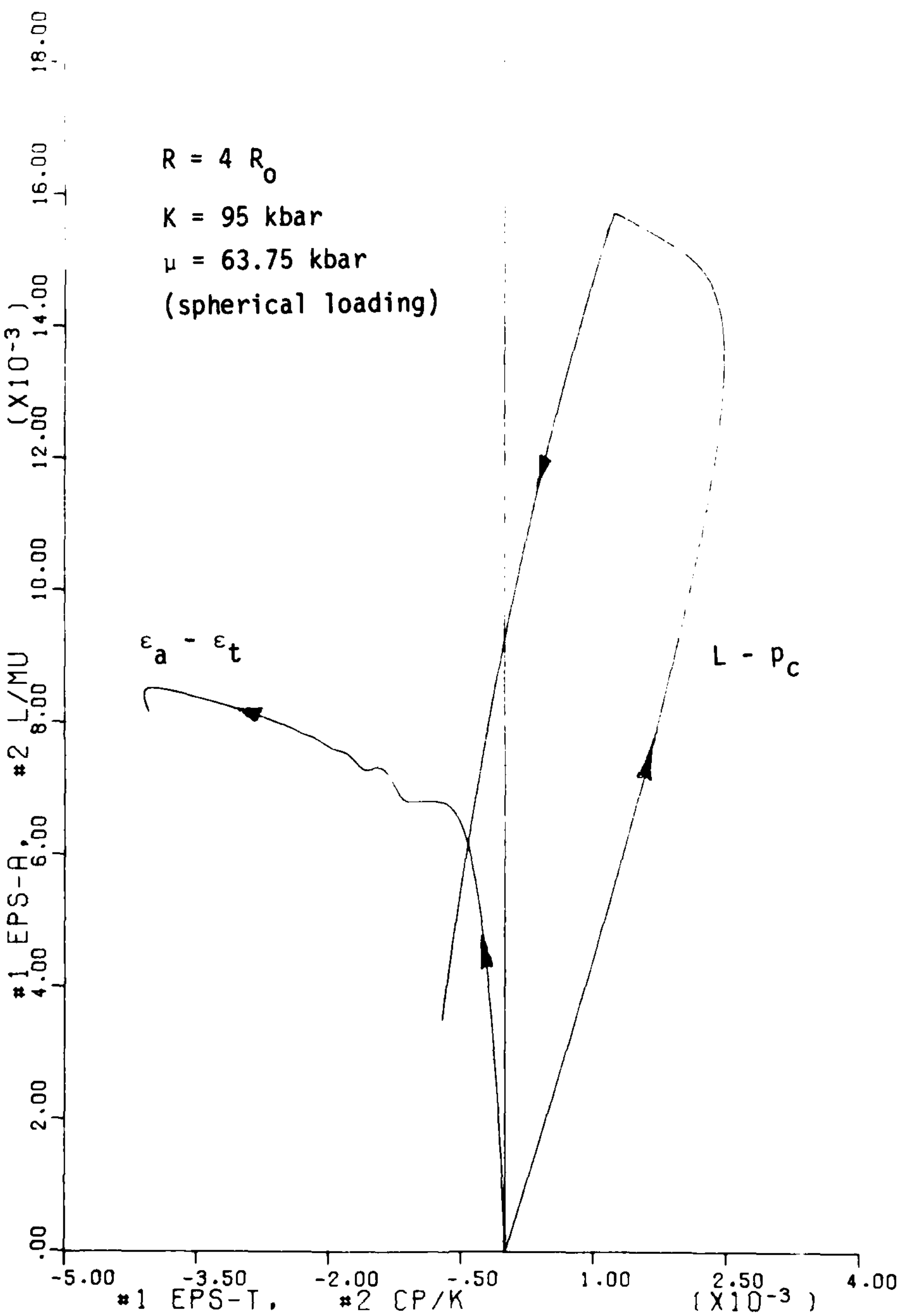

Figure 2d. Same as 2a, but with R = 4R_o. Note changes in vertical and horizontal scales.

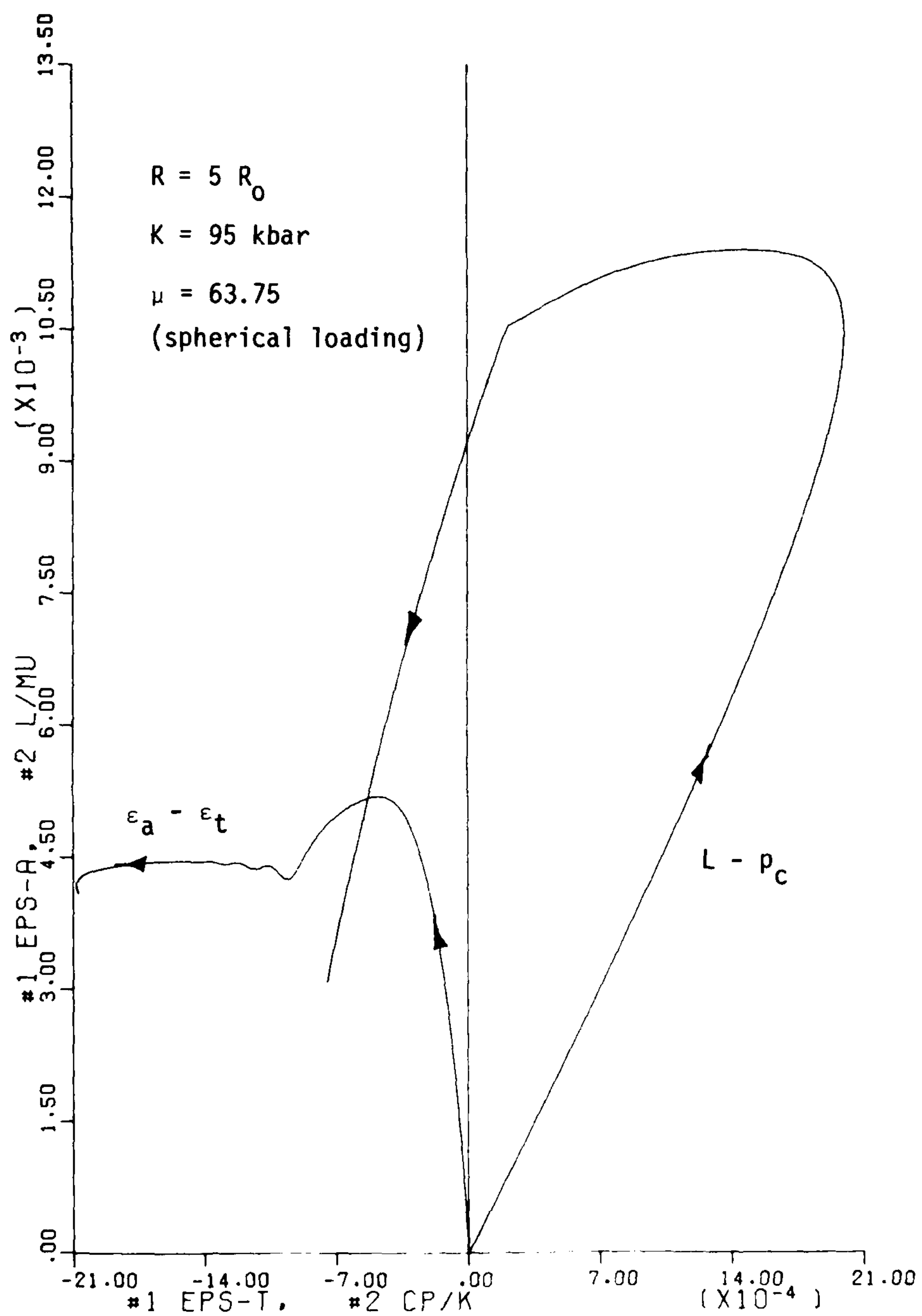

Figure 2e. Same as 2a, but with $R = 5R_0$. Note changes in vertical and horizontal scales.

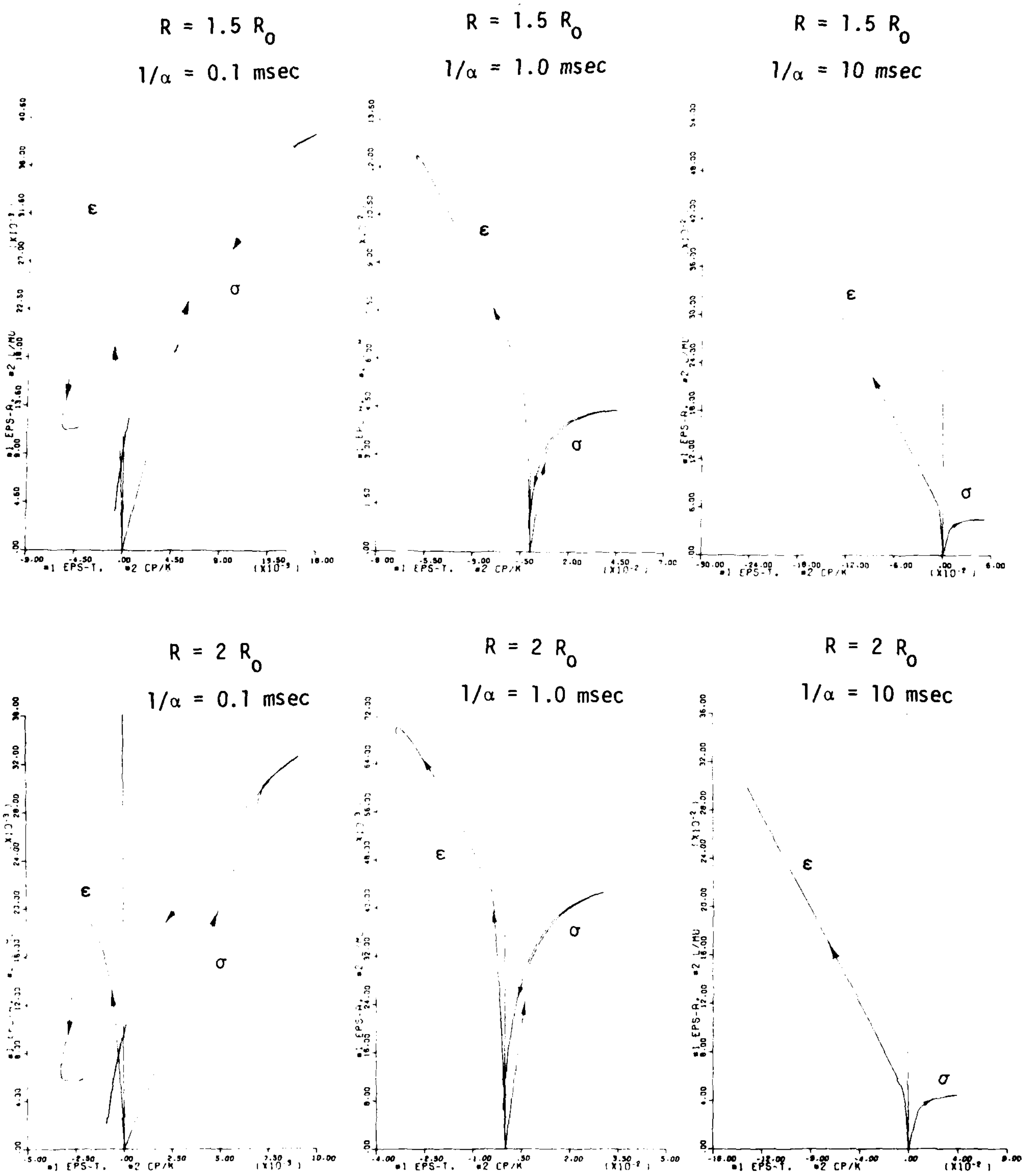

Figure 3. Strain paths and stress paths at various positions for cylindrical wave propagation in Mixed Company sandstone. A radial stress given by $\sigma_r = p_0 \exp(-\alpha t)$, with p_0 = 10 kbar and various values of $1/\alpha$, is applied at R_0 = 1m. Note changes in the vertical and horizontal scales in each graph.

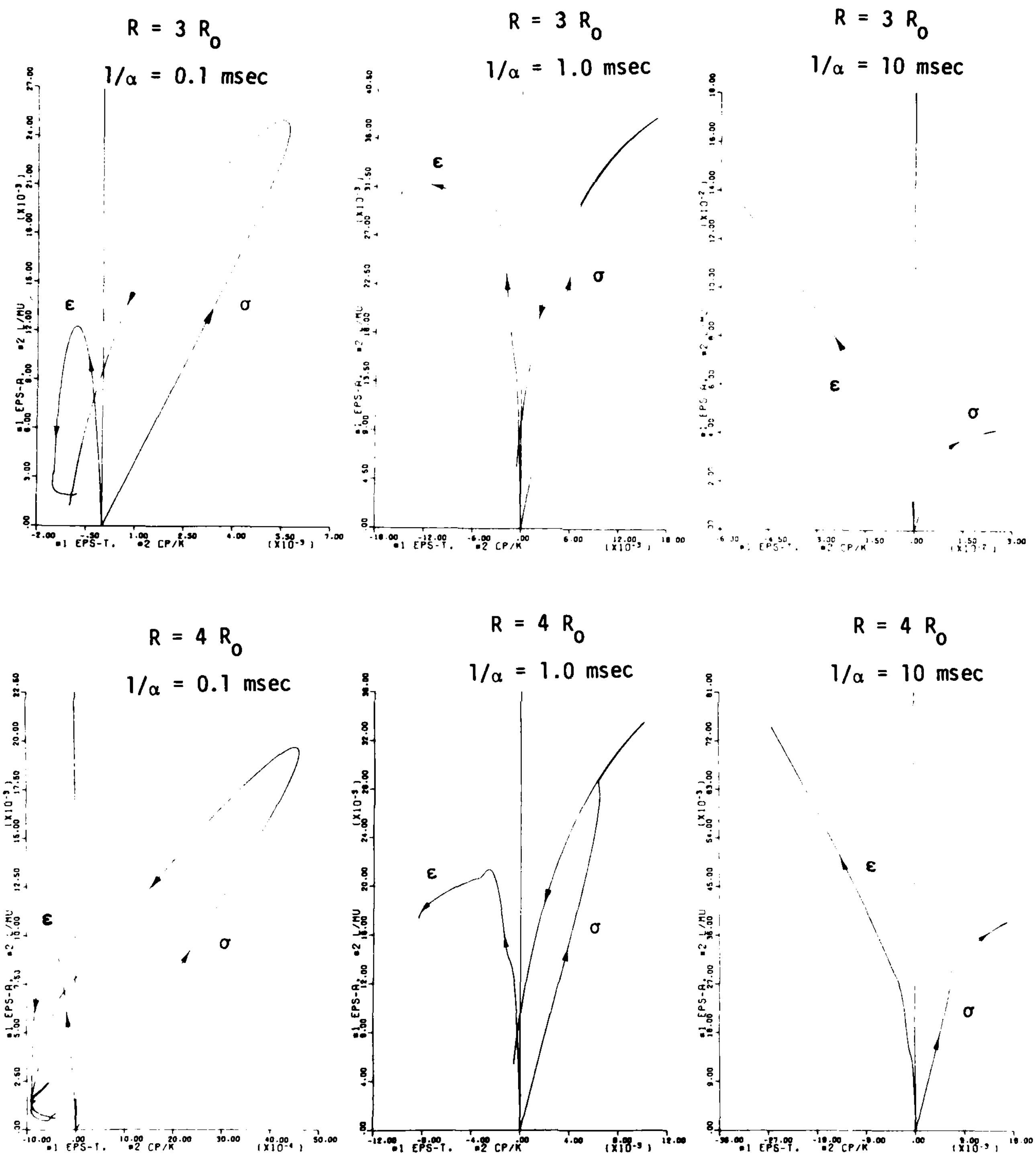

Figure 3. Continued.

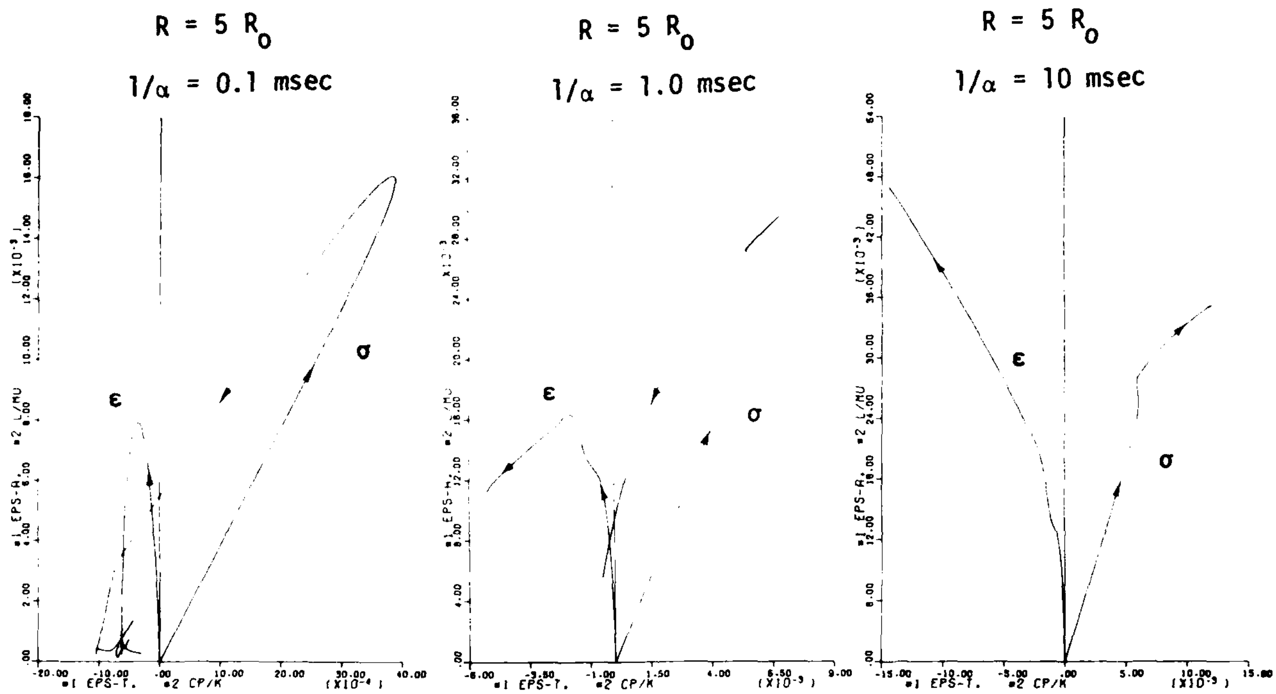

Figure 3. Continued.

STATIC EXPERIMENTAL SIMULATION OF LOAD-UNLOAD PATHS

Stress and strain paths were determined experimentally in the (L, p_c) and (ϵ_a, ϵ_t) planes using the results suggested by various one-dimensional finite-difference solutions given previously. A detailed discussion of experimental techniques used in these tests is presented in Appendix II. The stress and strain paths considered here correspond approximately to those given in Figure 3 for $R = 3R_0$ and three separate decay constants ($1/\alpha$ = 0.1 msec, 1.0 msec and 10 msec). Figures 4a, 4b and 4c show the three characteristic strain paths generated from the numerical solution and the strain paths to be followed in the static laboratory tests. The percent strains indicated here are used only to indicate orders of magnitude and are not the actual values achieved during testing. No attempt was made to follow the numerically determined strain paths exactly; they were used simply to indicate the *qualitative* nature of load-unload paths in the vicinity of buried explosions. Figure 4a shows the calculated and experimental paths corresponding to a decay time of $1/\alpha$ = 0.1 msec; this consists essentially of uniaxial-strain loading and constant-axial-strain unloading followed by uniaxial-strain unloading. Figure 4b shows the theoretical path corresponding to $1/\alpha$ = 10 msec in comparison to the experimentally followed path. The experimental strain path to be used consists of a uniaxial-strain loading and a constant-axial-strain unloading. Finally Figure 4c shows the theoretical path for $1/\alpha$ = 10 msec in comparison to the experimentally followed path. The experimental strain path to be used consists of uniaxial-strain loading and constant-volume-strain unloading. Kayenta sandstone from the Mixed Company site was the material tested in this investigation.

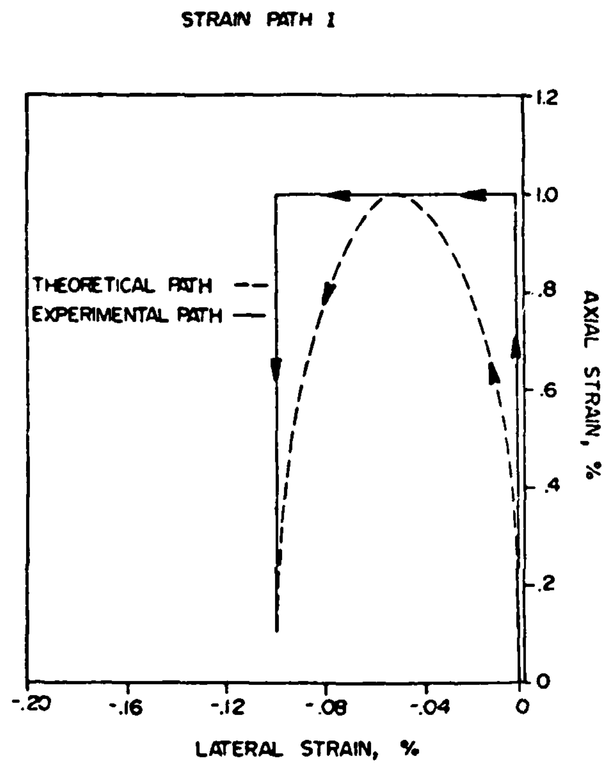

Figure 4a. Comparison of the theoretical (calculated) strain path to the experimental strain path to be followed during testing of path I ($1/\alpha$ = 0.1 msec). The experimental path shows a uniaxial-strain loading followed by a constant-axial and uniaxial-strain unloading. The percent strains indicated here are used only to indicate orders of magnitude and are not the actual values achieved during testing.

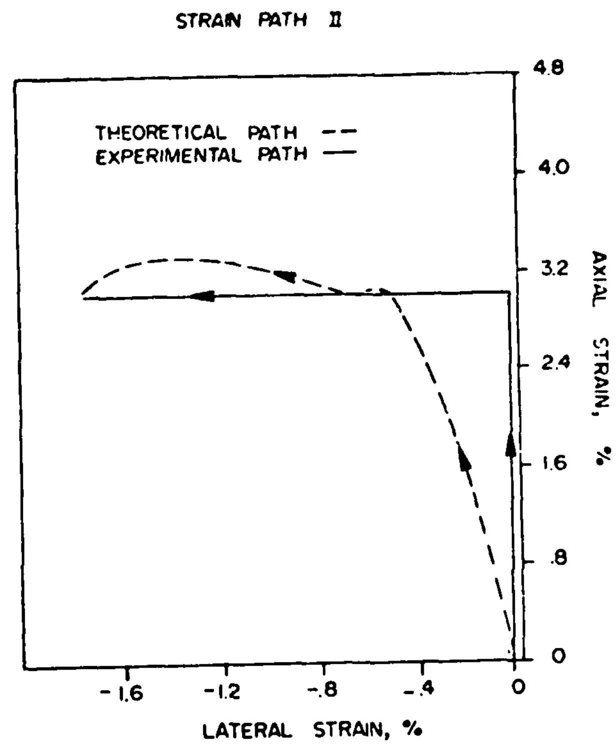

Figure 4b. Comparison of the theoretical (calculated) strain path to the experimental strain path to be followed during testing of path II ($1/\alpha$ = 1.0 msec). The experimental path shows a uniaxial-strain loading followed by a constant-axial-strain unloading. The percent strains indicated here are used to indicate orders of magnitude and are not the actual values achieved during testing.

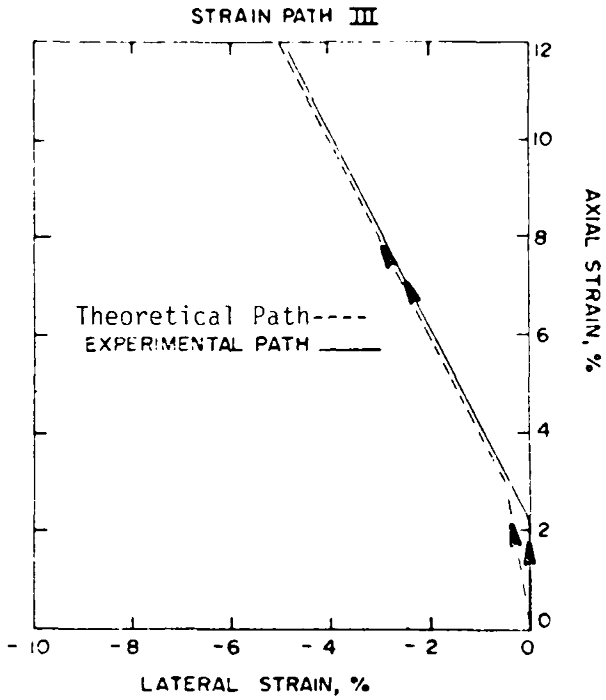

Figure 4c. Comparison of the theoretical (calculated) strain path to the experimental strain path to be followed during testing of path III ($1/\alpha$ = 10 msec). The experimental path shows a uniaxial-strain loading with a constant-volume-strain unloading. The percent strains indicated here are used only to indicate orders of magnitude and are not the actual values achieved during testing.

TEST RESULTS

The three strain paths, I, II and III, used in testing the Kayenta sandstone are shown in Figures 5a, 6a and 7a, respectively. Since all loading was conducted under uniaxial-strain conditions, a composite loading curve is shown for each path type. Individual unloading curves are shown for each test, departing from the composite loading curve at their respective maximum strains. The stress paths generated from the three strain paths are shown in Figures 5b, 6b and 7b. Composite loading curves are shown along with individual unloading curves. Included in each stress path figure is the triaxial failure envelope generated from this material. Tables I, II and III give computer listings for each test. Table Column 1 gives the data point while columns 2 through 8 give confining pressure (p_c) in kilobars, axial load ($\sigma_a - p_c$) in kilobars, axial strain (ε_a) in percent, the two transverse strains (ε_{t_1} and ε_{t_2}) in percent, volume strain ($\varepsilon_a + \varepsilon_{t_1} + \varepsilon_{t_2}$) in percent and mean stress $[1/3(\sigma_a + 2p_c)]$ in kilobars. All plots were constructed from these tables.

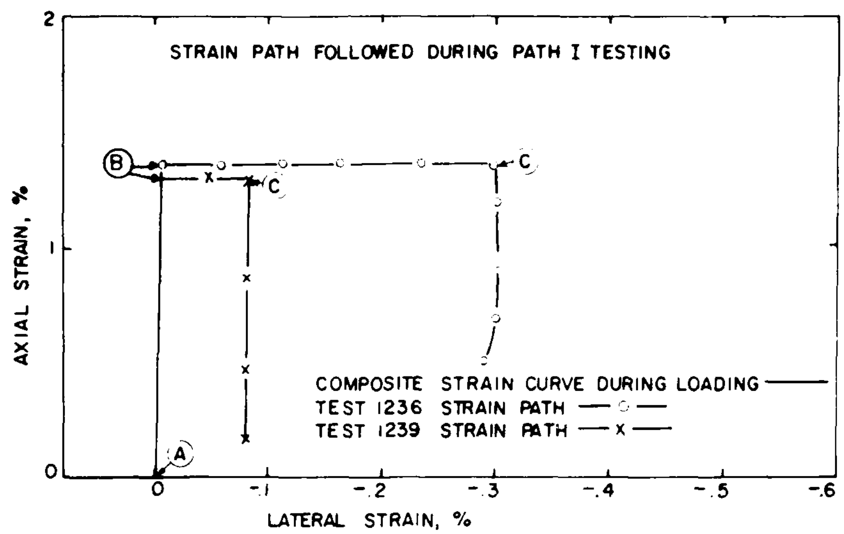

Figure 5a. Strain path followed during uniaxial-strain loading and constant-axial and uniaxial-strain unloading.

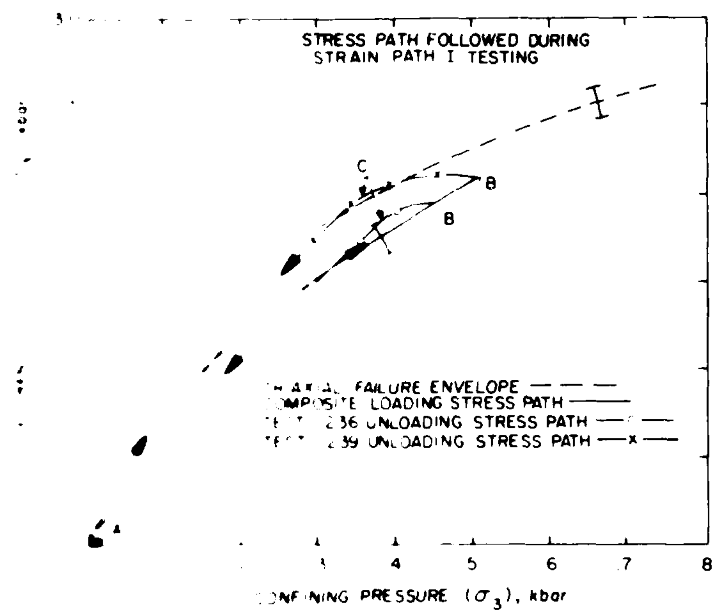

Figure 5b. Stress path followed during uniaxial-strain loading and constant-axial and uniaxial-strain unloading. The resulting stress path is a composite of four tests.

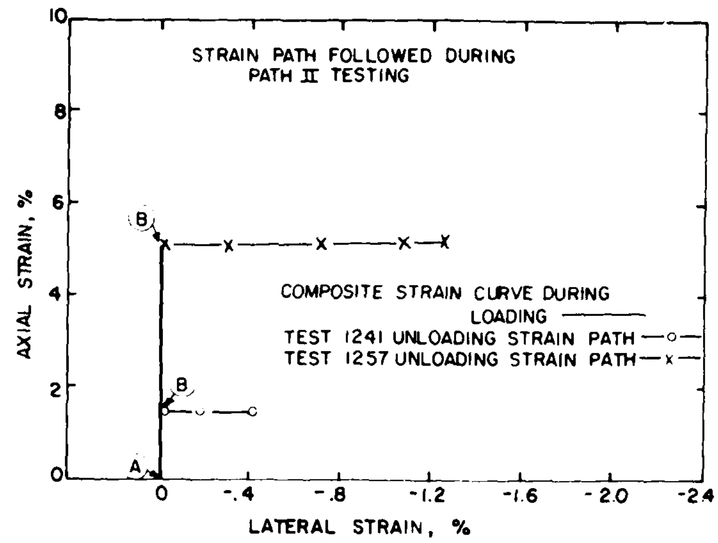

Figure 6a. Strain path followed during uniaxial-strain loading and constant-axial-strain unloading. The resulting stress path is a composite of four tests.

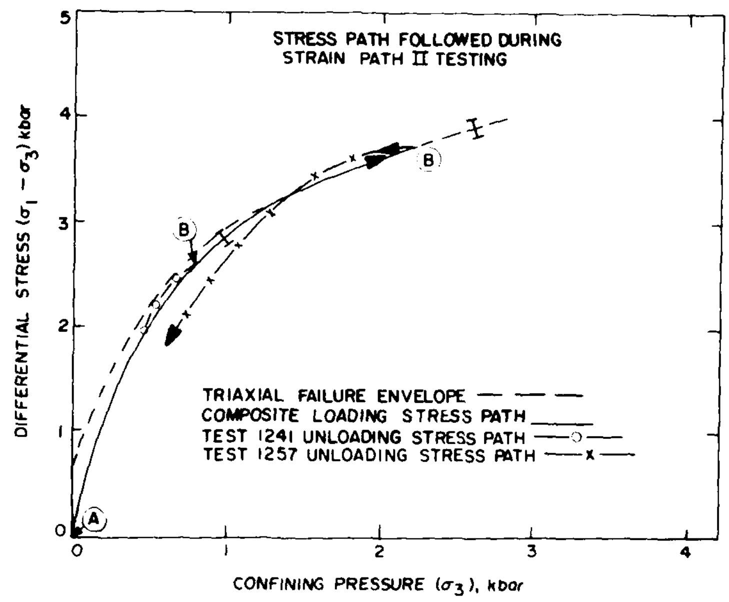

Figure 6b. Stress path followed during uniaxial-strain loading and constant-axial-strain unloading. The resulting stress path is a composite of four tests.

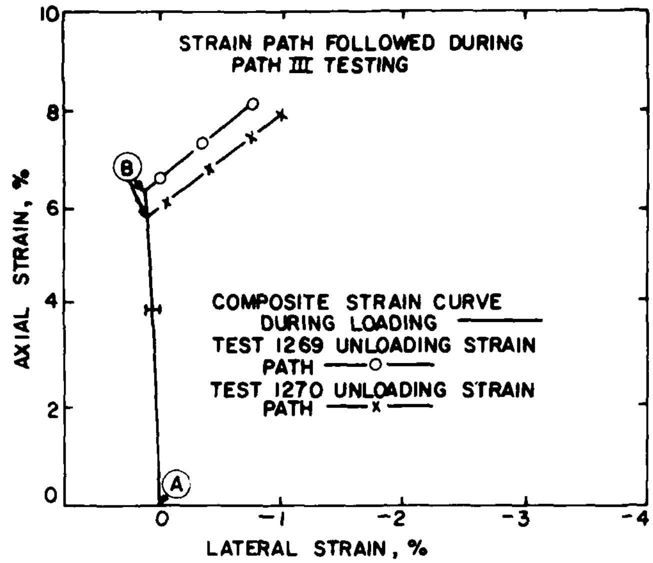

Figure 7a. Strain path followed during uniaxial-strain loading and constant-volume-strain unloading. The resulting stress path is a composite of three tests.

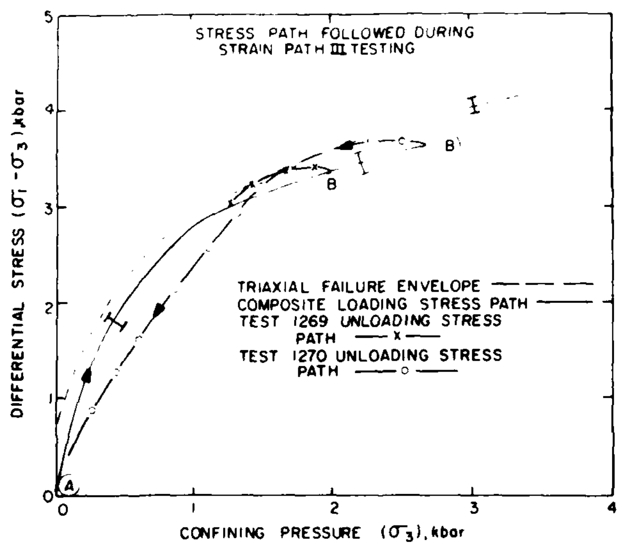

Figure 7b. Stress path followed during uniaxial-strain-loading and constant-volume-strain unloading. The resulting stress path is a composite of three tests.

TABLE Ia

1236 Test Results

Path Type I

N	CPRESS (KB)	LOAD (KB)	EA (%)	ET1 (%)	ET2 (%)	VOL STRAIN(%)	MEAN STRESS(KB)
1	0	- 589743E-3	- 198966E-2	- 227923E-2	386529E-2	- 403623E-3	- 196501E-3
3	83151E-2	121606	181541	282242E-1	- 249637E-1	184807	488504E-1
5	200948E-1	313309	309555	415941E-1	- 399487E-1	311206	124531
7	318745E-1	477203	40012	048219	- 504245E-1	397906	190942
9	595915E-1	728734	533219	571837E-1	- 613672E-1	529013	302503
11	789934E-1	86485	604486	572856E-1	- 067519	594191	367277
13	914661E-1	91214	633116	619089E-1	- 675545E-1	627434	395513
15	103246	949868	654895	632093E-1	- 660005E-1	652086	419868
17	121955	1 05335	708724	654594E-1	- 667998E-1	707375	473071
19	144821	1 16264	767839	641199E-1	- 711111E-1	760794	532367
21	173231	1 27378	824888	618403E-1	- 730928E-1	813543	597826
23	194019	1 3286	861657	654393E-1	- 068878	858188	636886
25	213421	1 36294	890641	684671E-1	- 682473E-1	890662	667733
27	235594	1 44635	938102	673253E-1	- 702074E-1	935393	717712
29	257075	1 48358	956794	703073E-1	- 660714E-1	961071	751601
31	283406	1 60262	1 02519	670041E-1	- 700385E-1	1 02213	817613
33	303501	1 6397	1 05002	674118E-1	- 694871E-1	1 04792	850069
35	334682	1 73746	1 10718	700496E-1	- 695377E-1	1 1077	913836
37	363093	1 80783	1 15244	681285E-1	- 700014E-1	1 15054	965702
39	392195	1 86739	1 19816	702766E-1	- 713021E-1	1 19712	1 01466
41	419912	1 93496	1 23929	664379E-1	- 716842E-1	1 23398	1 0649
43	437236	1 99076	1 27285	691269E-1	- 707975E-1	1 27116	1 10082
45	468417	2 02878	1 30454	719724E-1	- 686034E-1	1 30795	1 14468
47	48574	2 07371	1 33112	679377E-1	- 692227E-1	1 32982	1 17698
49	503063	2 12135	1 3576	686472E-1	- 705948E-1	1 35562	1 21018
* 51	466338	2 10998	- 249315	409562E-1	- 968951E-1	- 305106	1 16967
53	455252	2 11443	- 245639	030567	- 106806	- 321676	1 16006
55	442779	2 10519	- 24279	141534E-1	- 122558	- 350902	1 14451
57	454559	2 06011	- 238962	103141E-1	- 126253	- 354591	1 14126
59	424762	2 02492	- 230715	- 250156E-1	- 161672	- 416885	1 09974
61	398422	2 02259	- 212933	- 428723E-1	- 177985	- 453154	1 07263
63	375565	2 0114	- 237319	- 709826E-1	- 206743	- 514194	1 0527
65	363093	2 0113	- 238429	- 934331E-1	- 229259	- 560092	1 03353
67	348541	1 99372	- 237951	- 112404	- 247014	- 596192	1 01311
69	330525	1 87273	- 225585	- 217736	- 340219	- 781504	95477
71	309727	1 86271	- 22327	- 2391	- 362471	- 822595	930646
** 73	298651	1 7505	- 240055	- 195652E-1	- 929338E-1	- 352252	882149
75	275091	1 63442	- 291103	- 177727E-1	- 093062	- 401584	819899
77	257075	1 55954	- 317486	- 175714E-1	- 908614E-1	- 425546	776921
79	249453	1 49645	- 349849	- 158419E-1	- 899302E-1	- 455223	748269
81	223815	1 3761	- 403171	- 152192E-1	- 875477E-1	- 505497	682513
83	196791	1 24882	- 463275	- 198841E-1	- 925049E-1	- 575112	613065
85	178775	1 16965	- 50393	- 216118E-1	- 918012E-1	- 616739	568723
87	156601	1 05114	- 563114	- 203757E-1	- 913368E-1	- 674166	506982
89	139971	965498	- 604896	- 207744E-1	- 089296	- 71427	461804
91	124726	881336	- 654256	- 205561E-1	- 904281E-1	- 764484	418505
93	110175	808086	- 696613	- 217116E-1	- 090141	- 807656	379537
95	942378E-1	702826	- 752216	- 193822E-1	- 866764E-1	- 857449	328513
97	824581E-1	661027	- 785669	- 240526E-1	- 934877E-1	- 902251	3028
99	658279E-1	554337	- 84975	- 277209E-1	- 914351E-1	- 967858	250607
101	519694E-1	458078	- 914621	- 261378E-1	- 852149E-1	-1 02492	204662
103	415755E-1	350952	- 995999	- 110911E-2	- 583872E-1	-1 05489	158559
105	221736E-1	221945	-1 10572	- 032233	- 672505E-1	-1 20408	961552E-1

* Axial strain rezeroed for constant-axial-strain unloading.
** Lateral strains rezeroed for uniaxial-strain unloading.

TABLE Ib

1239 Test Results

Path Type I

N	CPRESS (KB)	LOAD (KB)	EA (%)	ET1 (%)	ET2 (%)	VOL STRAIN(%)	MEAN STRESS(KB)
1	0	- 58499E-3	- 206082E-2	- 227003E-2	384968E-2	- 48119E-3	- 194997E-3
3	194157E-1	873552E-1	156155	250928E-1	- 256204E-1	155626	485341E-1
5	360577E-1	293892	306155	272965E-1	- 254189E-1	308039	134022
7	540866E-1	473203	415595	030774	- 283919E-1	417986	211821
9	672615E-1	579115	473596	305865E-1	- 270049E-1	477195	2603
11	873707E-1	731595	548687	266409E-1	- 272188E-1	548106	331236
13	115801	87876	625928	282453E-1	- 254397E-1	628751	408721
15	144231	1 03537	712471	225723E-1	- 304202E-1	704567	489353
17	16434	1 08989	747505	261122E-1	- 253566E-1	748267	527637
19	19485	1 19804	811643	244489E-1	- 230615E-1	813041	594197
21	214266	1 23763	844662	227589E-1	- 231705E-1	844247	626808
23	24963	1 30836	899465	223023E-1	- 244658E-1	897282	685752
25	278061	1 42114	951811	242618E-1	- 226589E-1	953429	755107
27	305797	1 52818	1 01615	209592E-1	- 222701E-1	1 01482	815189
29	334227	1 62256	1 07606	176711E-1	- 257245E-1	1 06792	875081
31	358497	1 68145	1 1132	212868E-1	- 241623E-1	1 11029	918979
33	393168	1 75475	1 15822	218289E-1	- 216096E-1	1 15845	978085
35	428532	1 85241	1 22391	203977E-1	- 251594E-1	1 21909	1 046
37	463203	1 89597	1 25946	024394	- 233659E-1	1 26051	1 09519
39	492527	1 97146	1 3112	233009E-1	- 231568E-1	1 31135	1 14948
41	504808	1 95093	- 243433	024179	- 284393E-1	- 247682	1 15512
43	491633	1 94708	- 245324	186501E-1	- 032847	- 259486	1 14066
45	481926	1 94354	- 242887	170067E-1	- 436934E-1	- 269507	1 12977
47	457656	1 95222	- 244364	18922E-2	- 512623E-1	- 293612	1 1084
49	438934	1 95328	- 247528	- 120792E-1	- 677799E-1	- 327173	1 0900.
51	414664	1 94034	- 248153	- 371693E-1	- 896392E-1	- 374606	1 06144
53	392475	1 87085	- 246776	- 563056E-1	- 109498	- 412101	1 01609
55	366818	1 75782	- 303377	- 545605E-1	- 108634	- 46601	95276
57	335354	1 6171	- 372007	- 531126E-1	- 107597	- 532054	872566
59	[illegible]	1 5315	- 40.757	- 561851E-1	- 109581	- 568785	82221
61	288462	1 42397	- 45117	- 557297E-1	- 108176	- 614229	76 118
63	262112	1 31895	- 499867	- 521331E-1	- 107941	- 660071	70176
65	232988	1 20421	- 558467	- 523556E-1	- 11267	- 722503	63439
67	201785	1 0663	- 624899	- 547503E-1	- 110375	- 788924	557218
69	171968	97921	- 691578	- 544776E-1	- 1105	- 855747	485071
71	144231	8179	- 752791	- 535865E-1	- 112377	- 918415	416864
73	117881	701131	- 81912	- 520461E-1	- 111411	- 981172	351659
75	887575E-1	560162	- 90572	- 536127E-1	- 112354	-1 03012	275465
77	596339E-1	400782	-1 01419	- 504237E-1	- 114039	-1 17692	193228
79	409117E-1	286244	-1 09371	- 505246E-1	- 112486	-1 25488	136326
81	762768E-2	450468E-1	-1 38782	- 803057E-1	- 820593E-1	-1 54786	226432E-1

* Axial strains rezeroed for constant-axial-strain unloading.

TABLE IIa

1241 Test Results

Path Type II

N	CPRESS (KB)	LOAD (KB)	EA (%)	ET1 (%)	ET2 (%)	VOL STRAIN(%)	MEAN STRESS(KB)
1	0	20468E-1	- 115851E-1	- 444221E-2	172744E-2	- 142995E-1	682267E-4
3	689171E-2	199829E-1	5.1612	- 544431E-2	- 284666E-1	497523	202194E-1
5	172291E-1	173272	617116	- 594697E-2	- 281611E-1	582801	749865E-1
7	337694E-1	341891	661865	- 702541E-3	- 341489E-1	626785	147733
9	585795E-1	534208	707419	- 665779E-3	- 311719E-1	675358	236649
11	833897E-1	711335	775361	200558E-2	- 325259E-1	744608	320501
13	109578	812511	81791	- 865191E-3	- 384473E-1	77828	387089
15	171612	951752	818485	591716E-2	- 381901E-1	805742	442216
17	170225	1 06352	892077	- 38992E-2	- 379186E-1	849891	524733
19	195725	1 17792	915464	393981E-2	- 493035E-1	86969	588365
21	226717	1 26715	9668	194591E-2	- 495688E-1	918722	649122
23	261196	1 39452	1 01286	- 771885E-2	- 428018E-1	981819	726037
25	310816	1 47599	1 05029	- 80989E-1	- 040255	1 0088	802812
27	35492	1 59071	1 10847	446275E-2	- 374468E-1	1 07512	865167
29	38249	1 66146	1 13949	695887E-3	- 426404E-1	1 09708	956978
31	416949	1 76111	1 16718	- 81904E-2	- 508958E-1	1 10741	1 00399
33	452096	1 81294	1 18447	- 849354E-3	- 465508E-1	1 13651	1 05641
35	487911	1 91144	1 24501	- 833425E-2	- 451734E-1	1 19084	1 12575
37	542178	2 01021	1 28826	- 728086E-2	- 0445	1 27579	1 21245
39	589241	2 08199	1 32164	- 428[illegible]E-2	- 465[illegible]E-1	1 27015	1 28724
41	612659	2 15614	1 35214	- 770767E-2	- 428545E-1	1 3011	1 35117
43	660226	2 20456	1 3764	- 894762E-2	- 717262E-1	1 29504	1 39508
45	687104	2 2475	1 39905	- 516004E-2	- 470756E-1	1 4589	1 42627
47	705022	2 31125	1 41169	- 101416E-1	- 506607E-1	1 35004	1 47544
49	705022	2 [illegible]	1 39828	- 744009E-2	- 013880	1 35119	1 46283
51	[illegible]	2 32214	1 42212	- 126918E-1	- 451891E-1	1 36742	1 51006
53	[illegible]	2 32644	1 42709	- 456881E-2	- 131202E-1	1 37858	1 52941
55	774626	2 35801	1 4727	- 176879E-2	- 487865E-1	1 38032	1 56063
57	802195	2 41181	1 4878	- 821725E-2	- 411951E-1	1 41364	1 60617
59	8114	2 4106	1 48275	- 440993E-2	- 4 7856E-1	1 41384	1 64174
*61	[illegible]	2 40409	- 772759E-2	- 66007E-2	- 6 6827E-1	- 775985E-1	1 67801
63	[illegible]	2 44178	- 221775E-1	- 187167E-1	- 820571E-1	- 122904	1 6492
65	820114	2 42422	- 524431E-2	- 151419E-1	- 906896E-1	- 13101	1 62613
67	845301	2 41119	- 281662E-1	- 485168E-1	- 108582	- 185179	1 59901
69	76222	2 40781	588255E-2	- 791558E-1	- 14774	- 220898	1 56317
71	51147	2 36402	- 857948E-2	- 102076	- 185774	- 297161	1 5392
**	51271	2 0767	727181E-2	- 172174	- 261237	- 42648	1 2052

* Axial strain rezeroed for constant-axial-strain unloading.

** Sample failed due to jacket leak.

TABLE IIb

1257 Test Results

Path Type II

N	CPRESS (KB)	LOAD (KB)	EA (%)	ET1 (%)	ET2 (%)	VOL STRAIN(%)	MEAN STRESS(KB)
1	0	- 148644E-4	- 869849E-2	- 611251E-2	- 624006E-2	- 210496E-1	- 495481E-5
3	179088E-1	081949	1354	- 158112E-1	- 341167E-2	116152	452251E-1
5	365063E-1	24764	296826	- 012948	- 738807E-2	276431	119053
7	723239E-1	482886	44911	- 838544E-2	- 825744E-2	432393	233286
9	201129	1 10017	799277	- 009705	- 140653E-1	775318	567852
11	307204	1 38882	984475	- 573949E-2	- 01274	965814	770144
13	497313	1 87199	1 3003	- 794519E-2	- 194789E-1	1 27252	1 12131
15	546906	1 94803	1 35369	- 351501E-2	- 169373E-1	1 33296	1 19625
17	579969	2 04992	1 4176	- 514466E-2	- 188999E-1	1 39322	1 26328
19	680533	2 26515	1 56354	- 389695E-2	- 021617	1 53763	1 43558
21	725994	2 33251	1 61083	- 172212E-2	- 203504E-1	1 5884	1 5035
23	763189	2 40457	1 66431	- 261109E-2	- 247494E-1	1 6365	1 56471
25	789361	2 46736	1 70425	- 189321E-2	- 248209E-1	1 67708	1 61182
27	827936	2 50936	1 75592	121275E-2	- 233032E-1	1 73345	1 66439
29	885795	2 63541	1 84435	632482E-3	- 261527E-1	1 81836	1 76427
31	906459	2 68121	1 87655	- 178195E-2	- 269812E-1	1 84725	1 8002
33	92299	2 71291	1 90657	- 211972E-2	- 273343E-1	1 87655	1 82729
35	940899	2 73375	1 93109	- 494927E-3	- 023347	1 90679	1 85215
37	975339	2 74789	1 96086	610578E-2	- 234102E-1	1 94322	1 8911
39	1 02218	2 85366	2 042	256024E-2	- 262752E-1	2 0178	1 9734
41	1 04697	2 90255	2 09428	110712E-3	- 252145E-1	2 06866	2 01449
43	1 09657	2 93722	2 15461	251423E-2	- 222904E-1	2 13441	2 07564
45	1 16681	3 09442	2 31133	- 335846E-2	- 266806E-1	2 2806	2 1983
47	1 20678	3 11995	2 40735	- 205731E-2	- 240868E-1	2 38058	2 24676
49	1 2157	3 15545	2 50936	- 320668E-2	- 233136E-1	2 48217	2 28752
51	1 28254	3 17059	2 68972	- 729194E-2	- 220813E-1	2 65956	2 33941
53	1 31856	3 17925	2 83887	- 721278E-2	- 181939E-1	2 81274	2 37811
55	1 35969	3 19187	3 04567	- 111841E-1	- 185468E-1	3 01504	2 42431
57	1 58817	3 35091	3 77904	- 179652E-1	- 110108E-1	3 74897	2 70535
59	1 70684	3 41046	4 10266	- 216131E-1	- 870896E-2	4 07109	2 84366
61	1 93552	3 54502	4 48301	- 251071E-1	- 285185E-2	4 4538	3 1172
63	2 17247	3 67459	4 8432	- 298407E-1	- 429919E-2	4 81241	3 39734
65	2 29921	3 73457	5 018	- 284185E-1	323877E-3	4 9885	3 54407
67	2 38738	3 79133	5 11999	- 278413E-1	257092E-2	5 09343	3 65115
*69	2 30748	3 72977	- 335449	- 509426E-1	- 291423E-1	- 415249	3 55073
71	2 11114	3 75341	- 328219	- 116933	- 977041E-1	- 542037	3 38229
73	2 02369	3 71152	- 115904	- 156404	- 141204	- 612752	3 26086
75	1 77297	3 56977	- 291567	- 254155	- 240676	- 784345	2 96287
77	1 45612	3 28461	- 279294	- 407839	- 392585	-1 07589	2 55099
79	989115	2 65863	- 244605	- 835432	- 772266	-1 84192	1 87533
81	724616	2 13215	- 21141	-1 38836	-1 12775	-2 70838	1 43533
83	661911	1 80104	- 161892	- 117778	- 194421	- 475336	1 30626

* Axial strain rezeroed for constant-axial-strain unloading.

TABLE IIc*

1285 Test Results

Path Type II

N	CPRESS (KB)	LOAD (KB)	EA (%)	ET1 (%)	ET2 (%)	VOL STRAIN(%)	MEAN STRESS(KB)
1	0	- 383825E-3	- 389069E-2	- 003233	- 268728E-2	- 981065E-2	- 127942E-3
2	142881E-2	233706E-1	493756E-1	- 611584E-2	- 858556E-3	423979E-1	921902E-2
3	192889E-1	275378	358834	- 117936E-1	486112E-2	351877	111082
4	557226E-1	627454	586816	- 118582E-1	13665E-2	576263	264875
5	742982E-1	780215	687141	- 157566E-1	- 267323E-2	668585	33437
6	101446	891758	770969	- 131407E-1	- 916211E-3	756603	398698
7	122878	986647	847272	- 116234E-1	- 651835E-3	834893	45176
8	163599	1 10465	979892	- 789414E-2	694606E-3	932625	531817
9	185031	1 19009	1 01532	- 120042E-1	- 421043E-2	998943	581727
10	235039	1 34395	1 13342	- 012757	- 486564E-2	1 1156	683024
11	297193	1 55822	1 29577	- 178119E-1	- 116105E-1	1 26597	8166
12	409354	1 78856	1 50811	- 131252E-1	- 723151E-2	1 48744	1 00554
13	449361	1 90788	1 61017	- 160811E-1	- 959154E-2	1 58408	1 08532
14	477937	1 96145	1 65124	- 124604E-1	- 784195E-2	1 6306	1 13175
15	547949	2 10473	1 78364	- 180918E-1	- 911693E-2	1 75595	1 24953
16	610817	2 25015	1 90768	- 192815E-1	172829E-1	1 90575	1 36087
17	675113	2 37406	2 03607	- 195538E-1	- 85114E-2	2 00744	1 46647
18	72155	2 42902	2 09784	- 186077E-1	- 591604E-2	2 07281	1 53122
19	787275	2 53682	2 2117	- 196729E-1	- 291809E-2	2 18759	1 63288
20	840141	2 64091	2 32079	- 227172E-1	- 548768E-2	2 29194	1 72044
21	880148	2 67372	2 36269	- 196521E-1	- 977153E-3	2 34157	1 77139
22	924441	2 76093	2 46725	- 191488E-1	- 121856E-2	2 44638	1 84475
23	954446	2 80649	2 55319	- 0206-2	172149E-1	2 53217	1 88994
24	988117	2 86588	2 69752	- 255969E-1	- 263118E-2	2 66653	1 94403
25	1 0216	2 87923	2 81299	- 226248E-1	- 749808E-3	2 78793	1 98134
26	1 03103	2 88011	2 89016	- 249607E-1	- 143657E-2	2 863	1 99307
27	1 08018	2 90805	3 12882	- 208663E-1	- 163973E-2	3 10561	2 04953
28	1 16877	2 94881	3 6996	- 185413E-1	- 391603E-4	3 66034	2 17171
29	1 22715	3 00079	3 86908	- 199897E-1	- 143142E-2	3 84476	2 22748
30	1 31022	3 11091	4 28691	- 214228E-1	- 556425E-2	4 25879	2 36719
31	1 37594	3 11978	4 41419	- 227916E-1	- 848947E-2	4 38153	2 41587
32	1 5474	3 2516	4 99419	- 207557E-1	- 112912E-1	4 96055	2 63127
33	1 66171	3 35202	5 41754	- 213594E-1	- 129003E-1	5 38143	2 77905
34	1 78744	3 42621	5 84727	- 170119E-1	- 139484E-1	5 8145	2 92951
35	1 8646	3 48595	6 08785	- 181019E-1	- 135534E-1	6 05427	3 02658
36	1 99831	3 57148	6 47219	- 01704	- 123867E-1	6 44066	3 1894
37	2 10464	3 63866	6 72226	- 199912E-1	- 743502E-2	6 69299	3 31752
38	2 21037	3 67337	6 9364	- 196284E-1	- 623443E-2	6 90874	3 43483

* Showing only the uniaxial-strain loading.

TABLE IIIa

1269 Test Results

Path Type III

N	CPRESS (KB)	LOAD (KB)	EA (%)	ET1 (%)	ET2 (%)	VOL STRAIN (%)	MEAN STRESS (KB)
1	0	- 227e[illegible]2E-[illegible]	- 1[illegible]7[illegible]28E-2	- 8[illegible]1014E-3	229861E-2	982016E-4	- 758773E-4
2	276[illegible]36E-2	125848	237922	120078E-1	- 263284E-2	24732	447117E-1
3	621531E-2	174692	285465	225077E-1	585931E-2	313915	064446
5	131212E-1	31869	405245	218046E-1	418729E-2	431344	119418
7	276236E-1	530053	554722	253035E-1	759655E-2	587807	204308
9	415071E-1	679087	660527	250479E-1	131895E-1	699021	269869
11	571189E-1	792184	777519	209358E-1	128131E-1	772547	321447
13	759648E-1	877148	80249	285461E-1	250991E-1	856573	368414
15	966825E-1	958376	868751	250486E-1	366556E-1	941092	416141
17	114678	1 08569	977441	110885E-1	983331E-2	99857	476533
19	144[illegible]	1 18185	1 05755	148972E-1	192485E-1	1 09206	538951
21	17264[illegible]	1 28601	1 15098	174121E-1	224168E-1	1 18726	601316
23	19959	1 [illegible]	1 22479	141786E-1	287319E-1	1 26791	651141
25	229366	1 449[illegible]2	1 3076	145469E-1	314529E-1	1 35421	713073
27	266568	1 5[illegible]415	1 40511	186478E-1	416074E-1	1 46622	778016
29	301090	1 58767	1 55174	198122E-1	474344E-1	1 62204	828974
31	372174	1 68254	1 72451	016761	051432	1 79249	866353
[illegible]	[illegible]	[illegible]	[illegible]	98[illegible]192E-[illegible]	701618E-1	1 89947	901807
[illegible]	[illegible]	[illegible]	[illegible]	- 022677	10342	1 96015	928645
[illegible]	418447	1 85[illegible]21	1 94014	- 1[illegible]1277E-1	122941	2 02539	969568
[illegible]	48065	1 [illegible]	2 0589	- 604994E-1	161895	2 16241	1 05799
41	51517	1 80042	2 1444	- 749807E-1	175397	2 24699	1 11532
4[illegible]	560759	1 85[illegible]	2 20242	- 859071E-1	198158	2 34721	1 17942
45	591145	1 89[illegible]	2 24507	- 906984E-1	211712	2 41871	1 22246
4[illegible]	[illegible]	[illegible]	[illegible]	- 100065	229296	2 51292	1 27755
4[illegible]	6650[illegible]	[illegible]	2 44[illegible]	- 104209	242279	2 58771	1 31201
[illegible]	72[illegible]	2 0[illegible]	2 5[illegible]	- 110614	267596	2 72903	1 41415
[illegible]	756986	2 125[illegible]	2 6582	- 115259	2713	2 81845	1 46549
[illegible]	1 0248	2 40[illegible]	3 23449	- 142152	34527	3 50942	1 82604
[illegible]	1 [illegible]	[illegible]511	4 1 59[illegible]	- 149681	4077[illegible]4	4 39967	2 26036
[illegible]	1 [illegible]	[illegible]	4 844[illegible]	- 117[illegible]	42779	5 17014	2 72551
[illegible]	[illegible]	[illegible] 14145	5 79834	- 6[illegible]E-1	445788	6 20424	[illegible] 43538
[illegible]	2 71454	3 28114	6 28862	- 364187E-1	466799	6 74653	3 81326
*[illegible]5	2 16155	[illegible]	2 31174	- 991357	- 821076	465809	3 37845
[illegible]	2 09801	[illegible]	2 67585	-1 14482	-1 03432	450588	3 30971
[illegible]	2 04829	[illegible]	[illegible] 01069	-1 28996	-1 24108	420959	3 25697
[illegible]1	1 [illegible]	[illegible]	[illegible]	-1 44[illegible]	-1 45414	39812	3 17466
[illegible]	1 [illegible]	[illegible]	[illegible]	-1 [illegible]	-1 69969	361988	[illegible] 11952
112	1 69471	3 24448	4 1795	-1 7986	-1 9452	4357	2 7762
11[illegible]	1 55106	3 23787	4 2049	-1 7904	-1 95815	45635	2 62902
114	1 32876	2 8815	4 1946	-1 77718	-1 97792	42945	2 29886
115	1 27067	2 67918	4 1748	-1 7699	-1 98877	41632	2 12368
116	1 04417	[illegible]	4 189	-1 7565	-2 00702	42578	1 81858
117	879811	2 06[illegible]	4 146[illegible]	-1 74[illegible]	-2 02424	37833	1 57517
118	707854	1 86481	4 186	-1 72942	-2 04316	41342	1 32946
119	652298	1 69165	4 15	-1 72468	-2 04935	37897	1 21785
120	591145	1 5381	4 1427	-1 71918	-2 0566	36792	1 10391
121	721815	1 01614	4 0995	-1 69417	-2 08964	31574	66056

* Axial and lateral strains rezeroed for constant-volume unloading.

TABLE IIIb

1270 Test Results

Path Type III

N	STRESS (KB)	LOAD (KB)	EA (%)	ET1 (%)	ET2 (%)	VOL STRAIN(%)	MEAN STRESS(KB)
1	0	[illegible]	- 11941E-2	- 823014E-1	229861E-2	814884E-4	- 75877[illegible]E-4
[illegible]	[illegible]48754E-2	111099E-1	209[illegible]94	170057E-2	280152E-2	213905	719088E-2
[illegible]	[illegible]765E-2	666701E-1	260694	141636E-2	[illegible]20337E-2	265326	291677E-1
4	1[illegible]7404E-1	[illegible]1851	[illegible]22405	466983E-2	264551E-2	329744	940242E-1
5	265982E-1	400672	[illegible]89704	5[illegible]8373E-2	228105E-2	397398	162156
[illegible]	5[illegible]068E-1	6[illegible]58[illegible]4	4856[illegible]	811503E-2	241429E-2	496204	26232
[illegible]	104[illegible]	[illegible]145[illegible]	[illegible]	149729E-1	109218E-1	688[illegible]	409464
[illegible]	141[illegible]	1 0904	[illegible]145	13[illegible]E-1	01156	861182	507165
[illegible]	194[illegible]	1 [illegible]	[illegible]	15590[illegible]E-1	245674E-1	1 01048	614719
10	[illegible]947	1 50145	1 181[illegible]	216409E-1	412426E-1	1 24491	789954
11	400[illegible]	1 [illegible]	1 44[illegible]	256404E-1	638889E-1	1 5[illegible]776	1 01208
[illegible]	[illegible]	[illegible]	[illegible]	4990[illegible]E-1	857204E-1	2 36246	1 [illegible]1086
[illegible]	[illegible]	1 444[illegible]1	[illegible]	4[illegible]118[illegible]E-1	90[illegible]44E-1	2 442[illegible]4	1 [illegible]22
14	[illegible]	[illegible]	[illegible]	5[illegible]092E-1	945015E-1	2 [illegible]1917	1 42068
[illegible]	[illegible]	[illegible]	[illegible]141	6[illegible]8414E-1	9[illegible]3122E-1	[illegible] 00685	1 53664
[illegible]	441[illegible]	[illegible]	1[illegible]104	102175	[illegible]E-1	[illegible] 36705	1 70604
[illegible]	[illegible]	[illegible]	[illegible]514[illegible]	1111[illegible]4	[illegible]29464E-1	[illegible] 55259	1 [illegible]7924
[illegible]	[illegible]	[illegible]	[illegible]	1[illegible]	[illegible]15762E-1	[illegible] 86694	1 91[illegible]4
[illegible]	[illegible]	[illegible] 144	[illegible]	[illegible]	[illegible]	4 1574[illegible]	[illegible]
[illegible]	1	[illegible]	4 [illegible]	15[illegible]	[illegible]67096E-1	4 5[illegible]45	[illegible]
[illegible]	[illegible]	[illegible]	4 [illegible]	14[illegible]	1[illegible]2019	5 1154[illegible]	[illegible]
	1 [illegible]	[illegible]	4 [illegible]	14[illegible]14[illegible]	145151	5 272[illegible]	[illegible] 56602
	1 [illegible]	[illegible]	5 [illegible]	1 [illegible]	150416	5 [illegible]	[illegible]
[illegible]	1 [illegible]	[illegible]	5 [illegible]14	140505	16[illegible]	5 52069	[illegible] 71197
	1 [illegible]	[illegible]	[illegible]	141 [illegible]54	1[illegible]	5 62525	[illegible]
[illegible]	[illegible]	[illegible]	[illegible]	1 [illegible]	[illegible]	[illegible]	[illegible]
	1	[illegible]	5 44[illegible]	1 [illegible]	[illegible]	[illegible]	[illegible] 89201
[illegible]	[illegible]	1 [illegible]	[illegible]11	1 [illegible]514[illegible]	[illegible]129	6 05721	[illegible]
* [illegible]	[illegible]	[illegible]	[illegible]	1[illegible]	[illegible]	- 043567	[illegible] 841
[illegible]	1 [illegible]	1 [illegible]	4[illegible]14	11[illegible]	18581	- 512[illegible]28E-1	[illegible]784
	1 [illegible]	[illegible]	1 [illegible]14	[illegible]E-1	[illegible]	- 5[illegible]14[illegible]E-1	[illegible]
	1 [illegible]	[illegible]	11 [illegible]	[illegible]	[illegible]E-1	- [illegible]61948	[illegible]
[illegible]	1 [illegible]	[illegible]	[illegible]E-1	[illegible]E-1	11 [illegible]E-1	- [illegible]E-1	[illegible]
[illegible]	1 [illegible]	4	[illegible]	[illegible]	- 1 [illegible]	- [illegible]417[illegible]E-1	[illegible] 95146
[illegible]	1 [illegible]	[illegible]	[illegible]1	1 [illegible]	11[illegible]	- [illegible]	[illegible] 86[illegible]76
	1 [illegible]	[illegible]	[illegible]	- 41[illegible]	[illegible]	- [illegible]70569E-1	[illegible] 9057
[illegible]	1 [illegible]	[illegible]41	[illegible]	- [illegible]	[illegible]1 41	- [illegible]E-1	[illegible]
[illegible]	1 [illegible]	[illegible]	[illegible]4	[illegible]	[illegible]41	[illegible]51416E-1	[illegible] 4225
[illegible]	1 [illegible]	[illegible]44	1 [illegible]	[illegible]45 [illegible]	- [illegible]	- [illegible]E-1	[illegible]
[illegible]	1 [illegible]	[illegible]	1 [illegible]	- [illegible]	- [illegible]	- [illegible]	[illegible] 55172
** [illegible]	1 [illegible]	[illegible]	1 [illegible]	[illegible]	1 11[illegible]	- [illegible]	[illegible]1741

* Axial strain rezeroed for constant-volume unloading.

** Could not maintain constant volume path beyond this point.

TABLE IIIc*

1284 Test Results

Path Type III

N	CPRESS (KB)	LOAD (KB)	EM (%)	ET1 (%)	ET2 (%)	VOL STRAIN(%)	MEAN STRESS(KB)
1	0	- 376665E-2	- 388676E-2	- 32027E-2	- 26621E-2	- 975125E-2	- 125555E-3
2	854883E-2	622846E-1	75216	- 149543E-1	- 332151E-2	733747	293104E-1
3	121108E-1	102561	843309	- 104609E-1	- 186884E-1	832571	462986E-1
4	185225E-1	157061	944145	- 922923E-2	136395E-2	936206	708762E-1
5	292085E-1	262561	1 02428	- 647818E-2	258457E-2	1 01833	116729
6	051293	471617	1 17834	- 010468	56517E-2	1 17347	208499
7	641162E-1	594618	1 26195	- 128767E-1	- 284021E-2	1 24603	262322
8	961743E-1	754424	1 367	- 906736E-2	342316E-1	1 39251	347649
9	116064	957507	1 50469	- 160653E-2	- 899922E-3	1 50011	455238
10	186649	1 11871	1 62111	- 104691E-1	- 616456E-2	1 60443	559561
11	281399	1 38317	1 79088	- 851178E-2	- 592737E-2	1 77619	742522
12	3676	1 59402	1 93431	- 828092E-2	- 836621E-2	1 91734	698938
13	41884	1 78885	2 05618	- 927442E-2	- 109586E-1	2 03551	1 03512
14	537151	1 97243	2 17308	- 276544E-2	- 58837E-2	2 16424	1 19463
15	590582	2 11789	2 [illegible]	- 759998E-2	- 698865E-2	2 26061	1 29654
16	641877	2 1465	2 [illegible]814	- 2[illegible]5077E-2	- 651757E-2	2 32907	1 37404
17	644724	2 [illegible]274	2 49658	- 259106E-1	- 564952E-1	2 40188	1 42231
18	760846	2 496[illegible]2	2 66[illegible]1	- 170558E-1	- 255812E-1	2 60341	1 59295
19	815646	2 5[illegible]	2 6711[illegible]	- 417187E-1	- 256081E-2	2 6236	1 6621
20	85702	2 57834	2 71412	- 628936E-2	- 871633E-2	2 69871	1 71647
21	[illegible]	2 5641	2 72584	- 5[illegible]104E-2	- 908274E-2	2 71058	1 72409
22	91[illegible]	2 66566	2 84501	- 218[illegible]28E-2	- 442371E-2	2 83803	1 80685
23	975184	2 68011	2 88975	- 001285	- 208035E-2	2 88629	1 82882
24	971004	2 74416	2 91654	- 006014	- 290981E-2	2 92733	1 88579
25	996651	2 80212	3 1117	- 998059E-2	- 178352E-2	3 1175	1 93076
26	1 01[illegible]	2 8075	3 19294	- 872709E-2	141268E-2	3 18529	1 94683
27	1 02[illegible]	2 80477	3 22952	- 667084E-2	48245E-2	3 22761	1 95851
28	1 03512	2 80521	3 [illegible]	- 75403E-2	892217E-2	3 27379	1 9702
29	1 03939	2 80555	3 3158[illegible]	- 122741E-1	38966E-2	3 30717	1 97458
30	1 04509	2 80598	3 35291	- 141765E-1	628862E-2	3 34475	1 98042
31	1 05078	2 79574	3 39055	- 121592E-1	731786E-2	3 38555	1 98271
32	1 0550[illegible]	2 80674	3 43972	- 154218E-1	57038E-2	3 42966	1 99065
33	1 05644	2 80654	3 47717	- 165092E-1	425671E-2	3 46449	1 99211
34	1 06[illegible]	2 79118	3 49619	- 160671E-1	929616E-2	3 48916	1 99408
35	1 07217	2 78936	3 53316	- 011282	149368E-1	3 53488	2 00195
36	1 07[illegible]	2 80846	3 58804	- 200781E-1	00847	3 57602	2 01402
37	1 08641	2 8091	3 62114	- 202288E-1	865906E-2	3 61915	2 02278
38	1 09496	2 83909	3 67894	- 189082E-1	011578	3 67134	2 04132
39	1 10[illegible]	2 81472	3 71448	- 218222E-1	115284E-1	3 7238	2 05269
40	1 17618	2 89[illegible]21	4 10779	- 243971E-1	907738E-2	4 09184	2 14056
41	1 28569	2 97611	4 56412	- 170414E-1	190036E-2	4 54829	2 27792
42	1 39702	3 09107	4 94344	- 173613E-1	116768E-2	4 92645,	2 42738
43	1 48105	3 17198	5 18268	- 171149E-1	- 138257E-2	5 16323	2 53841
44	1 61074	3 25621	5 51801	- 113344E-1	- 19471E-3	5 50584	2 69614
45	1 [illegible]	3 30826	5 75472	- 221423E-2	900762E-2	5 76188	2 84173
46	1 85581	3 43943	6 03182	- 103145E-1	537705E-2	6 02658	3 00229
47	1 95269	3 53711	6 20585	- 106600E-1	747524E-2	6 20247	3 13173
48	2 12977	3 69382	6 56982	- 198083E-1	720997E-2	6 55639	3 36064
49	2 26[illegible]	3 76739	6 79175	- 169359E-1	112837E-1	6 78571	3 5191
50	2 38014	3 84504	6 96504	- 202929E-1	980456E-2	6 95382	3 66181
51	2 55111	3 96918	7 24433	- 228672E-1	113733E-1	7 23201	3 87417
52	2 70214	4 03322	7 45439	- 197335E-1	152866E-1	7 44961	4 04655
53	2 85602	4 1295	7 664	- 179739E-1	014452	7 66021	4 23252
54	2 90161	4 18075	7 75868	- 221236E-1	991314E-2	7 74553	4 2952
55	2 98995	4 23508	7 87622	- 189593E-1	109357E-1	7 86757	4 40164
56	3.00135	4 24656	7 9001	- 209629E-1	104262E-1	7 88873	4 41687

* Shows only the uniaxial-strain loading.

DISCUSSION AND CONCLUSIONS

An initial observation of the experimentally observed stresses indicates that there is little difference between the load-unload paths for strain path types II and III. Figures 6b and 7b suggest that if the yield condition is reached during uniaxial-strain loading with the stress paths following along the yield surface, then the unloading stress paths are similar in direction and magnitude for either constant-axial-strain or constant-volume-strain unloading. The numerial analysis solutions agree with the above observation in that regardless of the strain path, the stress path would follow along the yield surface during unloading (provided that yield was reached during uniaxial-strain loading). All of the experimentally observed stress paths show the unloading curve to go initially above and then cross through and go below the loading curve. The experimental unloading curves did not remain on or intersect (as in the case of strain path 2) the yield surface as illustrated by the numerical analysis.

Such variations in unloading material behavior may be modeled by including additional phenomena into the constitutive equations. Phenomena to be included in the equations would be permanent volume compaction and work-hardening of the shear failure envelope. The former effect will mainly influence the strain paths and the latter will change the stress paths, particularly in the unloading portion. It was experimentally determined that the material behaved nonlinearly during initial loading as compared to the linear model used in the numerical analysis. Such nonlinearities may be also handled by the aforementioned considerations. The observation that the unloading path lies below the loading path in stress space may be related to fracture and the resulting loss of cohesion, rather than ductile plastic flow, as asumed in the calculations.

Inclusion of pore pressure effects into the model would be of interest in future work. Both the calculations and laboratory strain-path tests should be performed under various saturation conditions. Much of the previous theoretical work, including the finite-difference computer code, already contains this capability; it has just not been exercised yet. Also of future interest would be some theoretical results for two-dimensional dynamic loading situations, expressed in terms of ε_a, ε_t, L and p_c. This could be done by calculating the following invariants as functions of time at a particular material element:

$$\tau(t) = \left\{(1/6)[(\sigma_{11}-\sigma_{22})^2 + (\sigma_{22}-\sigma_{33})^2 + (\sigma_{33}-\sigma_{11})^2] + \sigma_{12}^2 + \sigma_{13}^2 + \sigma_{23}^2 \right\}^{1/2} , \qquad (14)$$

$$p(t) = (\sigma_{11} + \sigma_{22} + \sigma_{33})/3 , \qquad (15)$$

$$\varepsilon_v(t) = \varepsilon_{11} + \varepsilon_{22} + \varepsilon_{33} , \qquad (16)$$

$$\varepsilon_d(t) = \left\{(1/6)[(\varepsilon_{11}-\varepsilon_{22})^2 + (\varepsilon_{22}-\varepsilon_{33})^2 + (\varepsilon_{33}-\varepsilon_{11})^2] + \varepsilon_{12}^2 + \varepsilon_{13}^2 + \varepsilon_{23}^2 \right\}^{1/2} . \qquad (17)$$

The desired quantities used for comparison with laboratory tests are then obtained from Eqs. (9) - (12).

The results presented here have shown that

(1) We can define strain paths for static testing of rock (and soil) samples that are more representative of actual field situations that those commonly used heretofore in constitutive modeling, and that

(2) It is possible to reproduce these paths in laboratory tests.

APPENDIX I

General Relationships and Finite-Difference Calculations

The equation for momentum conservation in Eulerian coordinates is given by

$$-\rho \dot{v} = \frac{\partial \sigma_r}{\partial r} + (g-1)\,\frac{\sigma_r - \sigma_\theta}{r} \quad , \tag{18}$$

where ρ is the material density, v is the radial particle velocity, σ_r and σ_θ are the radial and tangential stress components, and g is 1 (for plane flow), 2 (for cylindrical flow) or 3 (for spherical flow). A dot over a variable indicates time differentiation at a fixed material element and r is the Eulerian spatial coordinate. It is inconvenient to deal with Eulerian coordinates, hence we choose to express Eq. (18) in terms of Lagrangian coordinates representing the initial configuration. We define R as the initial radial coordinate of a material element whose current radial location is at r. Radial and transverse stress components in the initial configuration (Lagrangian) are denoted σ_R and σ_Θ. If the initial density is given by ρ_o, then mass conservation requires that

$$\rho_o R^{g-1}\, dR = \rho r^{g-1}\, dr \quad . \tag{19}$$

If the *forces* on a material element are to be the same in the two representations, then

$$R^{g-1}\, \sigma_R = r^{g-1}\, \sigma_r \quad , \tag{20}$$

$$\sigma_\Theta\, dR^{g-1} = \sigma_\theta\, dr^{g-1} \quad . \tag{21}$$

Now write Eq. (18) as

$$-\rho r^{g-1}\, dr\, \dot{v} = d(r^{g-1}\sigma_r) - \sigma_\theta\, dr^{g-1} \quad , \tag{22}$$

keeping in mind that the differentials on the right-hand side are taken at constant time. Substitution of Eqs. (19) - (21) into Eq. (22) then gives

$$-\rho_o R^{g-1}\, dR\, \dot{v} = d(R^{g-1}\sigma_R) - \sigma_\Theta dR^{g-1} \quad , \tag{23}$$

or

$$-\rho_o \dot{v} = \frac{\partial \sigma_R}{\partial R} + (g-1)\,\frac{\sigma_R - \sigma_\Theta}{R} \quad , \tag{24}$$

in Lagrangrian coordinates.

In order to use Eq. (24) in a finite-difference solution, an artificial viscous stress q is included. The following equations, with the addition of a constitutive law, then form the basis of the numerical calculations:

$$\rho_o \dot{v} = \frac{\partial \sigma_R}{\partial R} - (g-1)\,\frac{(\sigma_R - \sigma_\Theta)}{R} - \frac{\partial q}{\partial R} \tag{25}$$

$$\begin{aligned} q &= \rho_o A^2\, (\Delta R)^2\, \left|\frac{\partial v}{\partial R}\right|^2 \;, \quad \frac{\partial v}{\partial R} \leq 0 \\ &= 0 \quad , \quad \frac{\partial v}{\partial R} > 0 \end{aligned} \tag{26}$$

$$\dot{\varepsilon}_R = -\frac{\partial v}{\partial R} \quad , \quad \dot{\varepsilon}_\Theta = -\frac{v}{R} \quad , \tag{27}$$

where A is nondimensional constant on the order of unity, ΔR is the spatial increment in the finite-difference solution, and $\dot{\varepsilon}_R$ and $\dot{\varepsilon}_\Theta$ are the radial and tangential strain rates in the initial configuration. A straight-forward centered difference scheme is used and Eqs. (25) - (27) are written in finite-difference form as

$$\rho_o \frac{v_j^{i+\frac{1}{2}} - v_j^{i-\frac{1}{2}}}{\Delta t} = - \frac{(\sigma_R)^i_{j+\frac{1}{2}} - (\sigma_R)^i_{j-\frac{1}{2}}}{\Delta R} -$$

$$(g-1) \frac{(\sigma_R)^i_{j+\frac{1}{2}} + (\sigma_R)^i_{j-\frac{1}{2}} - (\sigma_\Theta)^i_{j+\frac{1}{2}} - (\sigma_\Theta)^i_{j-\frac{1}{2}}}{2R_j}$$

$$- \frac{q^{i-\frac{1}{2}}_{j+\frac{1}{2}} - q^{i-\frac{1}{2}}_{j-\frac{1}{2}}}{\Delta R} \quad , \qquad (28)$$

$$(\dot{\varepsilon}_R)^{i+\frac{1}{2}}_{j+\frac{1}{2}} = \frac{v_j^{i+\frac{1}{2}} - v_{j+1}^{i+\frac{1}{2}}}{\Delta R} \quad , \qquad (29)$$

$$(\dot{\varepsilon}_\Theta)^{i+\frac{1}{2}}_{j+\frac{1}{2}} = - \frac{v_j^{i+\frac{1}{2}} + v_{j+1}^{i+\frac{1}{2}}}{2R_{j+\frac{1}{2}}} \qquad (30)$$

The stress rates ($\dot{\sigma}_R$ and $\dot{\sigma}_\Theta$) are obtained from $\dot{\varepsilon}_R$ and $\dot{\varepsilon}_\Theta$, and therefore the stresses and strains are calculated from

$$X^{i+1}_{j+\frac{1}{2}} = X^i_{j+\frac{1}{2}} + \dot{X}^{i+\frac{1}{2}}_{j+\frac{1}{2}} \Delta t \quad , \qquad (31)$$

where X represents σ_R, σ_Θ, ε_R and ε_Θ.

The constitutive model used here is expressed in terms of the principal stress and strain components σ_i and ε_i (i = 1, 2 and 3) with the following identification:

$g = 1$ (Plane Flow):

$$\dot{\varepsilon}_1 = -\partial v/\partial R \quad , \quad \dot{\varepsilon}_2 = \dot{\varepsilon}_3 = 0$$

$$\sigma_1 = \sigma_R, \quad \sigma_2 = \sigma_3 = \sigma_Z$$

$g = 2$ (Cylindrical Flow)

$$\dot{\varepsilon}_1 = -\partial v/\partial R \quad , \quad \dot{\varepsilon}_2 = -v/R \quad , \quad \dot{\varepsilon}_3 = 0$$

$$\sigma_1 = \sigma_R \quad , \quad \sigma_2 = \sigma_\Theta \quad , \quad \sigma_3 = \sigma_Z$$

$g = 3$ (Spherical Flow):

$$\dot{\varepsilon}_1 = -\partial v/\partial R \quad , \quad \dot{\varepsilon}_2 = \dot{\varepsilon}_3 = -v/R$$

$$\sigma_1 = \sigma_R \quad , \quad \sigma_2 = \sigma_3 = \sigma_\Theta \quad .$$

Let us define the volume strain ε_v, the mean stress p, the stress deviators s_i and the second invariant of the stress tenser according to

$$\varepsilon_v = \varepsilon_1 + \varepsilon_2 + \varepsilon_3 \quad , \tag{32}$$

$$p = (\sigma_1 + \sigma_2 + \sigma_3)/3 \quad , \tag{33}$$

$$s_i = \sigma_i - p \quad , \tag{34}$$

$$J_2 = (s_1^2 + s_2^2 + s_3^2)/2 \quad . \tag{35}$$

The elastic-plastic constitutive relation used here is then defined according to the following equations:

$$p = \hat{p}(\varepsilon_v) \quad , \tag{36}$$

$$\dot{s}_i = 2\mu(\dot{\varepsilon}_i - \dot{\varepsilon}_v/3) - 2\mu\xi\frac{s_i}{\sqrt{J_2}} \quad . \tag{37}$$

The variable ξ is determined by the condition that the stress state must remain on the failure surface, defined by

$$\sqrt{J_2} = f(p) \quad , \tag{38}$$

when a material element is undergoing plastic deformation.

From Eq. (35) we find that

$$2\sqrt{J_2}\,\dot{\sqrt{J_2}} = s_i\dot{s}_i \quad \text{(Summation)} \tag{39}$$

and

$$\dot{\sqrt{J_2}} = (\mu/\sqrt{J_2})\, s_i\dot{\varepsilon}_i - 2\mu\xi = f'(p)\dot{p} \quad . \tag{40}$$

Therefore, the variable ξ in Eq. (37) is given by

$$2\mu\xi = (\mu/\sqrt{J_2})\, s_i\dot{\varepsilon}_i - f'(p)\dot{p} \quad , \tag{41}$$

or, in terms of σ_i and p, as

$$2\mu\xi = (\mu/\sqrt{J_2})(\sigma_i\dot{\varepsilon}_i - p\dot{\varepsilon}_v) - f'(p)\dot{p} \quad . \tag{42}$$

If it is desired to include effects of fluid saturation defined by nonzero pore pressure p_p, σ_i is replaced by the effective stress components $\langle\sigma_i\rangle \equiv \sigma_i - nP_p$ $(0 < n < 1)$ in the elasticity relationship and by $\sigma_i^* \equiv \sigma_i - P_p$ in the failure surface relationship:

$$\langle p\rangle = p - nP_p = \hat{p}(\varepsilon_v) \quad , \tag{43}$$

$$\langle \dot{s}_i \rangle = \dot{s}_i = 2\mu(\dot{\varepsilon}_i - \dot{\varepsilon}_v/3) - 2\mu\xi \frac{s_i}{\sqrt{J_2}} \quad , \tag{44}$$

$$2\mu\xi = (\mu/\sqrt{J_2})(\sigma_i\dot{\varepsilon}_i - p\dot{\varepsilon}_v) - f'(p^*)(1-m)\dot{p} \quad , \tag{45}$$

where

$$m \equiv \frac{dP_p}{dp} \quad . \tag{46}$$

The function f(p) is taken to be of the form

$$f(p) = S_o + \Delta S(1 - e^{-p/a}) \quad . \tag{47}$$

Analytical Determination of Elastic Stress and Strain Paths for a Spherical Explosion

If u(r,t) is the radial displacement, the spherical wave equation for purely elastic deformation can be written as

$$\partial^2 u/\partial t^2 = c^2[\partial^2 u/\partial r^2 + (2/r)\, \partial u/\partial r - (2/r^2)u] \quad , \tag{48}$$

where r is the radial coordinate, t is the time and c is the longitudinal elastic wave speed. This expression takes a simpler form if it is written in terms of a displacement potential Ψ such that

$$u(r,t) = c^2 \partial/\partial r\, (\Psi/r) \quad . \tag{49}$$

In this case

$$\partial^2\Psi/\partial t^2 = c^2\, \partial^2\Psi/\partial r^2 \quad , \tag{50}$$

whose solution for outgoing waves is given by the familiar expression

$$\Psi = \Psi(t - \frac{r - r_o}{c}) \quad . \tag{51}$$

The displacement, strain components and stress components can be expressed in terms of Ψ and its derivatives Ψ' and Ψ'' according to

$$u(r,t) = -(c/r)\Psi' - (c/r)^2 \Psi \quad , \tag{52}$$

$$-\varepsilon_a = \partial u/\partial r = (1/r)\Psi'' + (2c/r^2)\Psi' + (2c^2/r^3)\Psi \quad , \tag{53}$$

$$-\varepsilon_t = u/r = -(c/r^2)\Psi' - (c^2/r^3)\Psi \quad , \tag{54}$$

$$-\sigma_a = (1/r)\ [(\lambda+2\mu)\Psi'' + (4\mu c/r)\Psi' + (4\mu c^2/r^2)\Psi] \quad , \tag{55}$$

$$-\sigma_t = (1/r)\ [\lambda\Psi'' - (2\mu c/r)\Psi' - (2\mu c^2/r^2)\Psi] \quad , \tag{56}$$

where λ and μ are the Lamé constants. The sign convention used throughout this work is that stresses and strains are positive in compression. For a pressure history at $r = r_o$ given by

$$\left.\begin{aligned} \sigma_r(r_o,t) &= 0 \quad , && t < 0 \\ \sigma_r(r_o,t) &= p_o e^{-\alpha t} \quad , && t \geq 0 \end{aligned}\right\} \tag{57}$$

The function Ψ must satisfy the following ordinary differential equation:

$$(\lambda+2\mu)\Psi''(t) + (4\mu c/r_o)\Psi'(t) + (4\mu c^2/r_o^2)\Psi(t) = -r_o p_o e^{-\alpha t} \quad , \tag{58}$$

subject to the conditions, from Eqs. (52) and (58), that jumps in Ψ and Ψ' at $t = 0$ obey the following relationships:

$$\left.\begin{aligned} (\lambda + 2\mu)\ [\Psi'] + (4\mu c/r_o)\ [\Psi] &= 0 \quad , \\ [\Psi'] + (c/r_o)\ [\Psi] &= 0 \quad , \end{aligned}\right. \tag{59}$$

where [ ] indicates the jump in the function, i.e., $[f] = f(0^+) - f(0^-)$. Equations (59) thus require that Ψ and Ψ' each be continuous at $t = 0$ as long as $\lambda \neq 2\mu$. Hence, a solution to Eq. (58) can be written as

$$\Psi(t) = e^{-\beta_2 t} (M \cos \beta_1 t + N \sin \beta_1 t) + \Psi_0 e^{-\alpha t} \quad , \tag{60}$$

where

$$M = -\Psi_0 = \frac{r_0 p_0}{\alpha^2(\lambda+2\mu) - 4\mu c\alpha/r_0 + 4\mu c^2/r_0^2} \quad , \tag{61}$$

$$N = \frac{\alpha r_0 (\lambda+2\mu) - 2\mu c}{2c \sqrt{\mu(\lambda+\mu)}} \Psi_0 \quad , \tag{62}$$

$$\beta_1 = \frac{2c \sqrt{\mu(\lambda+\mu)}}{r_0 (\lambda+2\mu)} \quad , \tag{63}$$

$$\beta_2 = \frac{2\mu c}{r_0 (\lambda+2\mu)} \quad . \tag{64}$$

In the case of an elastic fluid $\mu = 0$ and the displacement potential and its first two derivatives become

$$\Psi = \frac{r_0 p_0}{\lambda \alpha^2} (1 - e^{-\alpha t} - \alpha t) \quad , \tag{65}$$

$$\Psi' = \frac{r_0 p_0}{\lambda \alpha} (e^{-\alpha t} - 1) \quad , \tag{66}$$

$$\Psi' = - \frac{r_0 p_0}{\lambda} e^{-\alpha t} \quad . \tag{67}$$

If $\alpha = 0$ (i.e., the cavity pressure remains constant at p_0) in the case of a fluid, the displacement potential and its first two derivatives become

$$\Psi = -\frac{r_o p_o}{2\lambda} t^2 \quad , \tag{68}$$

$$\Psi' = -\frac{r_o p_o}{\lambda} t \quad , \tag{69}$$

$$\Psi'' = -\frac{r_o p_o}{\lambda} \quad . \tag{70}$$

In the special case of spherical wave propagation we can make the identification that $L = \sigma_a - \sigma_t$ and $p_c = \sigma_t$, in which case the stress and strain paths can be written parametrically as

$$L = -(2\mu/r)[\Psi'' + (3c/r)\Psi' + (3c^2/r^2)\Psi] \quad , \tag{71}$$

$$p_c = -(1/r)[\lambda\Psi'' - (2\mu c/r)\Psi' - (2\mu c^2/r^2)\Psi] \quad , \tag{72}$$

$$\varepsilon_a = -(1/r)[\Psi'' + (2c/r)\Psi' + (2c^2/r^2)\Psi] \quad , \tag{73}$$

$$\varepsilon_t = (c/r^2)[\Psi' + (c/r)\Psi] \quad . \tag{74}$$

Equations (71) to (74) in the case of spherical elastic waves are the analytical counterparts of Eqs. (9) to (12) for numerical solutions. Comparison of strain and stress paths calculated by the two methods is shown in Figure 8 for $1/\alpha = 1$ msec, $R/R_o = 3$, $K = 95$ kbar, $c = 3$ km/sec, and $\rho_o = 2.0$ gm/cm^3. It can be seen that the numerical solution gives a good approximation of the strain and stress paths except for the peak values associated with the main compressive fronts. This is a result of the viscous stresses that are included in the finite-difference solution to damp out numerical oscillations, and has no significance with regard to the conclusions reached in this report.

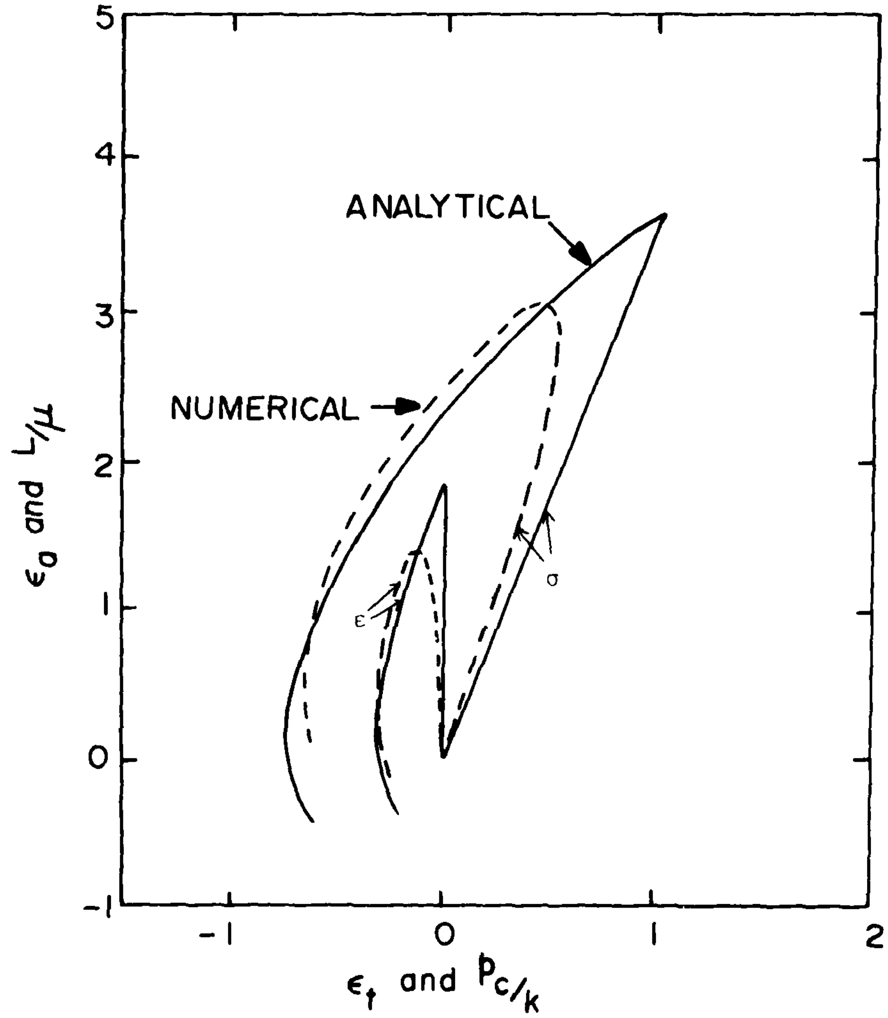

Figure 8. Comparison of strain and stress paths determined numerically and analytically for spherical wave propagation in an elastic medium.

APPENDIX II

EXPERIMENTAL TECHNIQUE

Specimen Preparation

Specimens were prepared from Kayenta sandstone, Mixed Company Site. Cylindrical samples 3.81 centimeters long by 1.91 centimeters diameter were used thus maintaining a length to diameter ratio of 2 to 1. Specimen ends were ground parallel to within ± .001 centimeters. Specimens were air dried with weight, length and diameters being recorded for each sample for use in determining sample density and strains. Samples were prepared for testing by first wrapping them in urethane plastic (.025 cm thick) with hardened steel endcaps attached at each end using stainless steel lock wire.

Stress and Strain Determination

Stress and strain transducers were placed within the pressure vessel. Confining pressure was measured using a calibrated 350-ohm manganin pressure sensitive coil accurate to ± .003 kbars. Jacketed samples were placed and centered on the load cell when in the pressure vessel. The load cell was accurate to ± .005 kbars. Axial and lateral strain transducers were of the cantilever type using strain gauges in a wheatstone bridge configuration to obtain voltage output. The axial cantilevers measured total axial displacement and were calibrated to be accurate to ± .003 percent strain. Lateral strain cantilevers were positioned at mid-sample and sampled strains at 90 degree intervals. Diametrically opposed arms were calibrated for lateral strain. The lateral strains were averages with a resulting accuracy of ± .006

percent. Figure 9 shows a schematic of the transducers when inside the pressure vessel. Further discussion on transducer design may be obtained in Terra Tek report TR 75-29.

Testing Procedures

Seven samples were first tested triaxially to failure to generate the triaxial failure envelope for the material while eight samples were tested following the three strain paths. Triaxial testing commenced by first hydrostatically loading the samples to the desired confining pressure with subsequent axial loading to failure, stresses and strains being recorded during all phases of loading. A strain rate of about 10^{-4} sec^{-1} was used during loading.

Uniaxial-strain loading was used when following a specified strain path. Axial load and confining pressure were applied such that zero lateral strain was maintained. When following strain path I, II or III during unloading, i.e., constant-axial-strain and uniaxial-strain unloading, constant axial strain unloading and constant volume strain unloading, respectively, the confining pressure and axial load were adjusted to maintain the desired strain state.

Data Acquisition and Analysis

Both x-y recorders and a PDP Lab 11 computer were used for data acquisition. The x-y recorders were used primarily for instantaneous feedback during testing while the PDP Lab 11 computer data was used for analysis of pressure effects, endcap effects and generation of stress and strain load-unload curves. Tables I, II and III presented in the text are a result of the computer analysis.

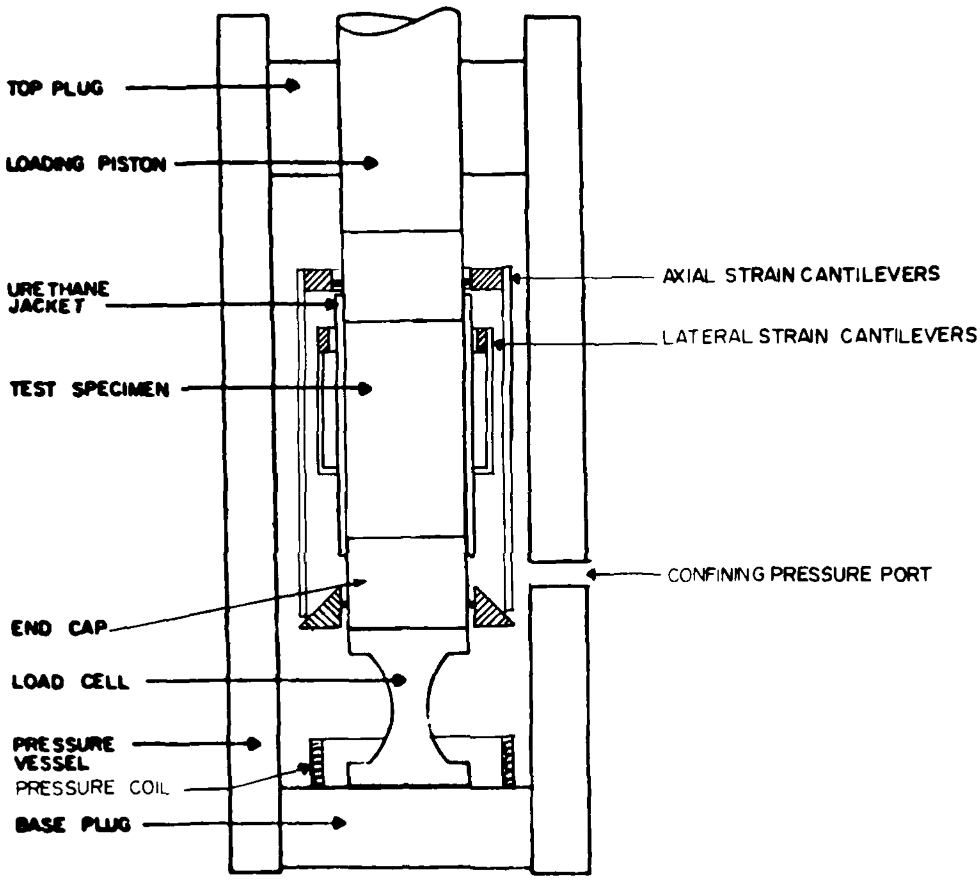

Figure 9. Pressure vessel schematic showing the sample and stress and strain transducers.

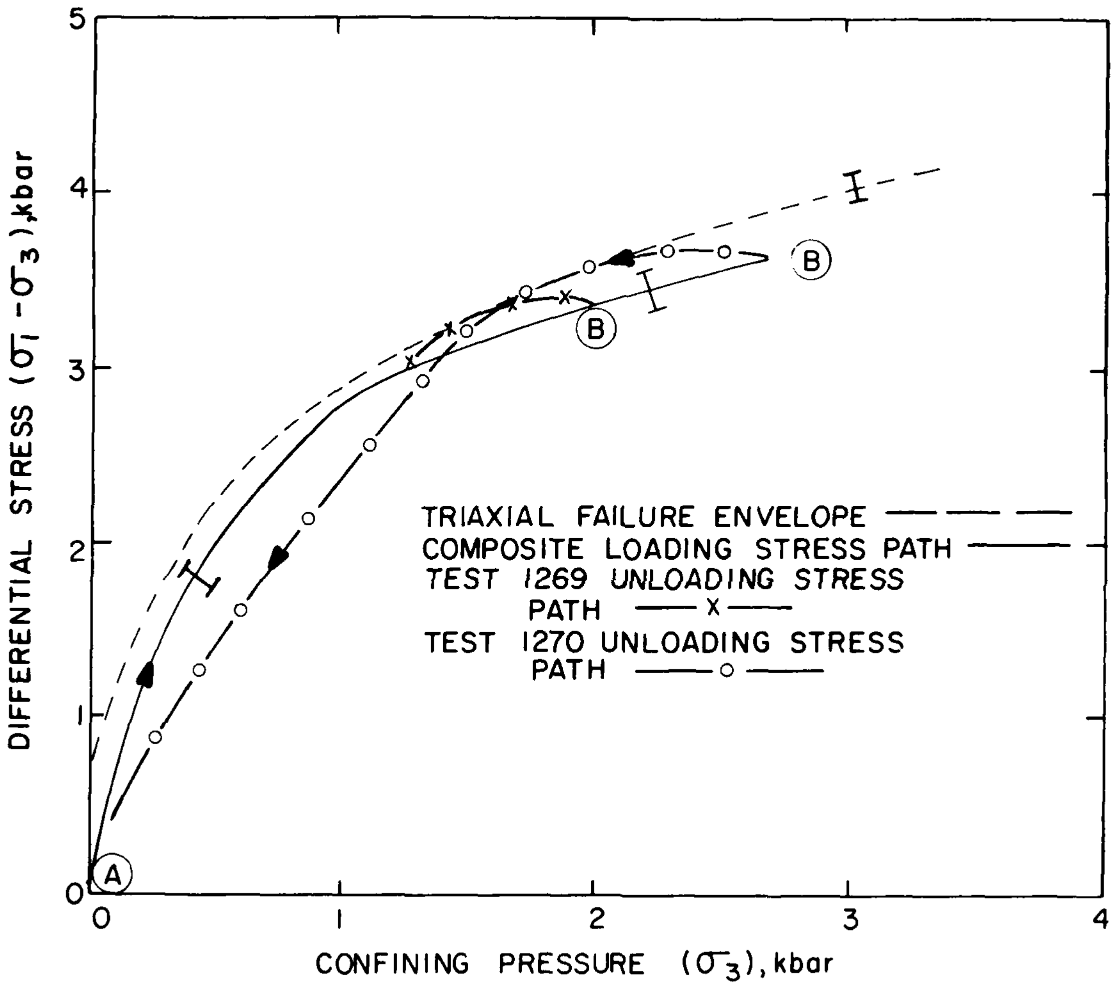

Figure 9a. Stress path followed during strain path III testing.

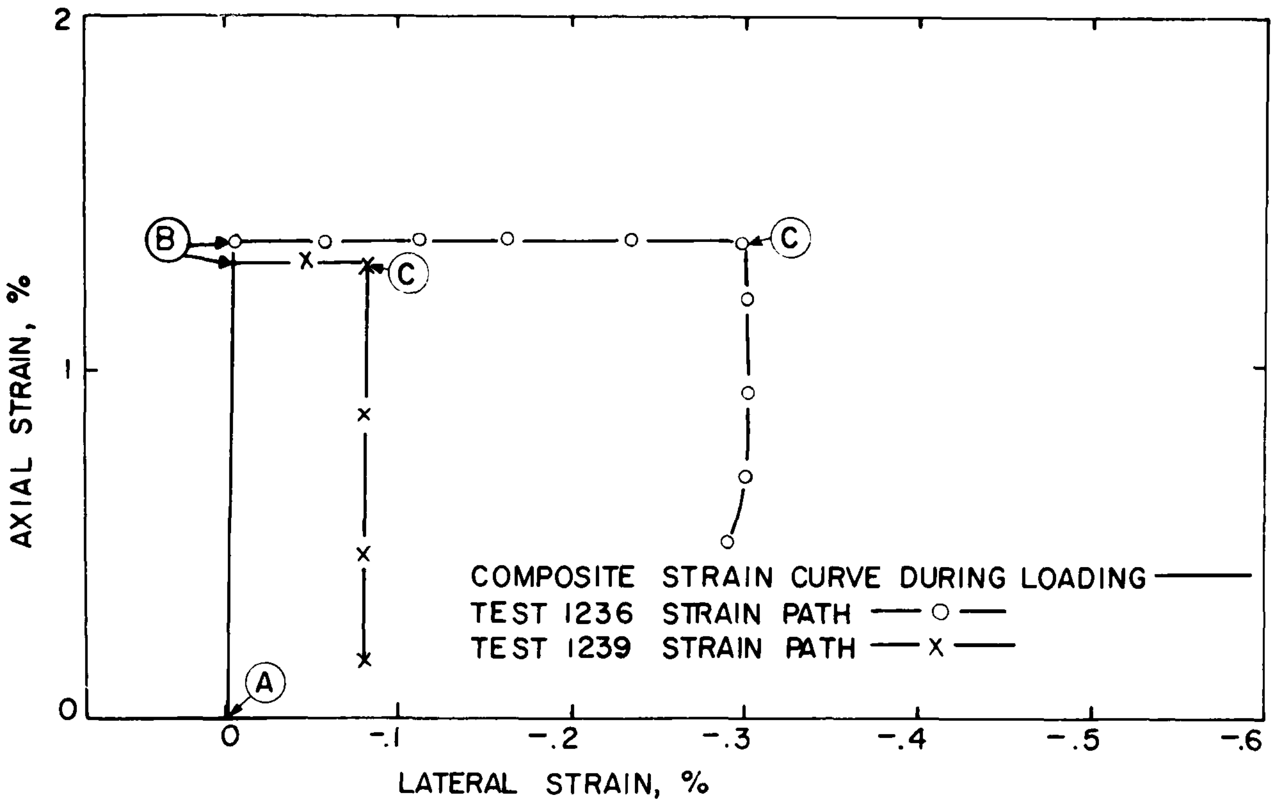

Figure 9b. Strain path followed during path I testing.

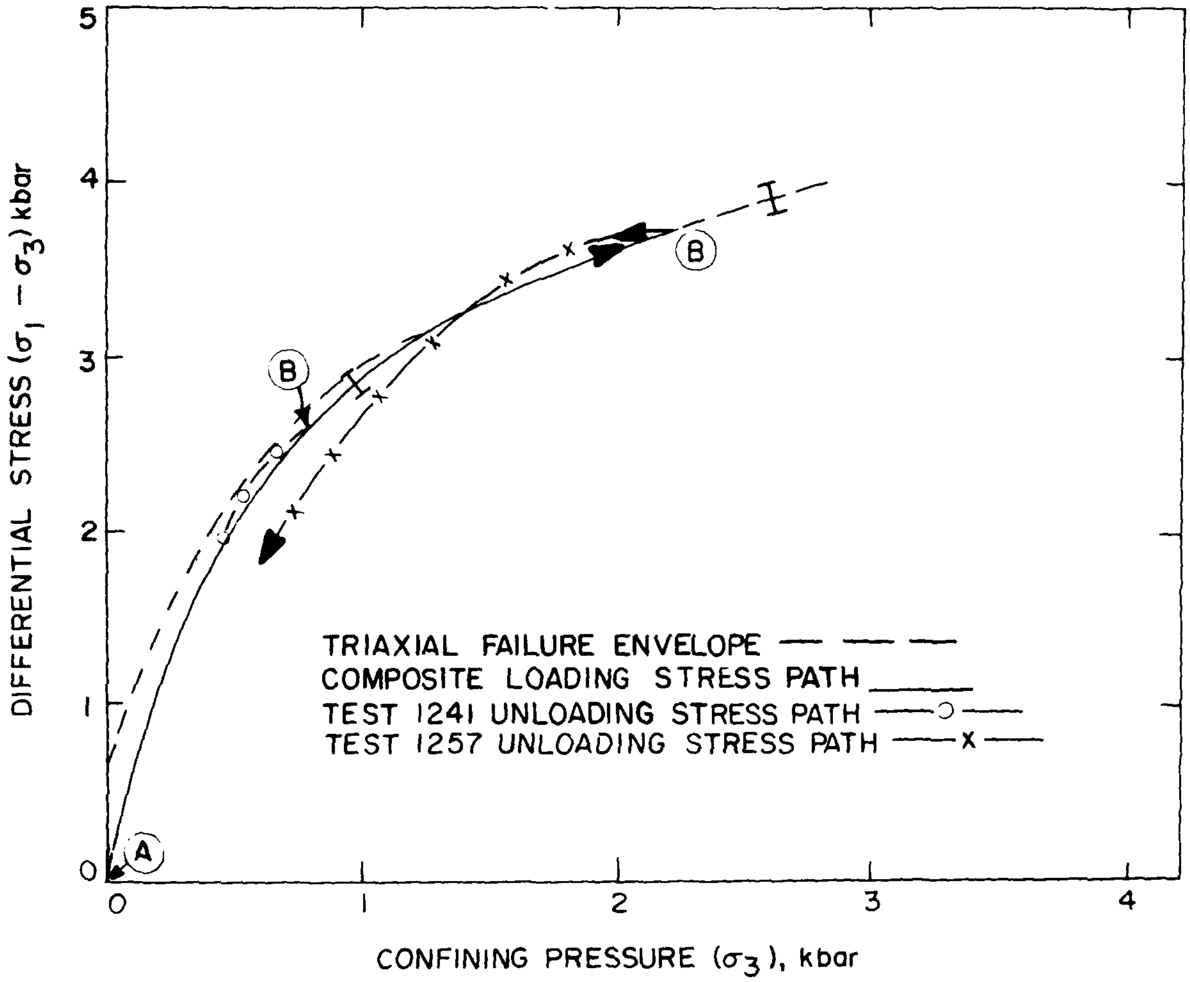

Figure 9c. Stress path followed during strain path II testing.

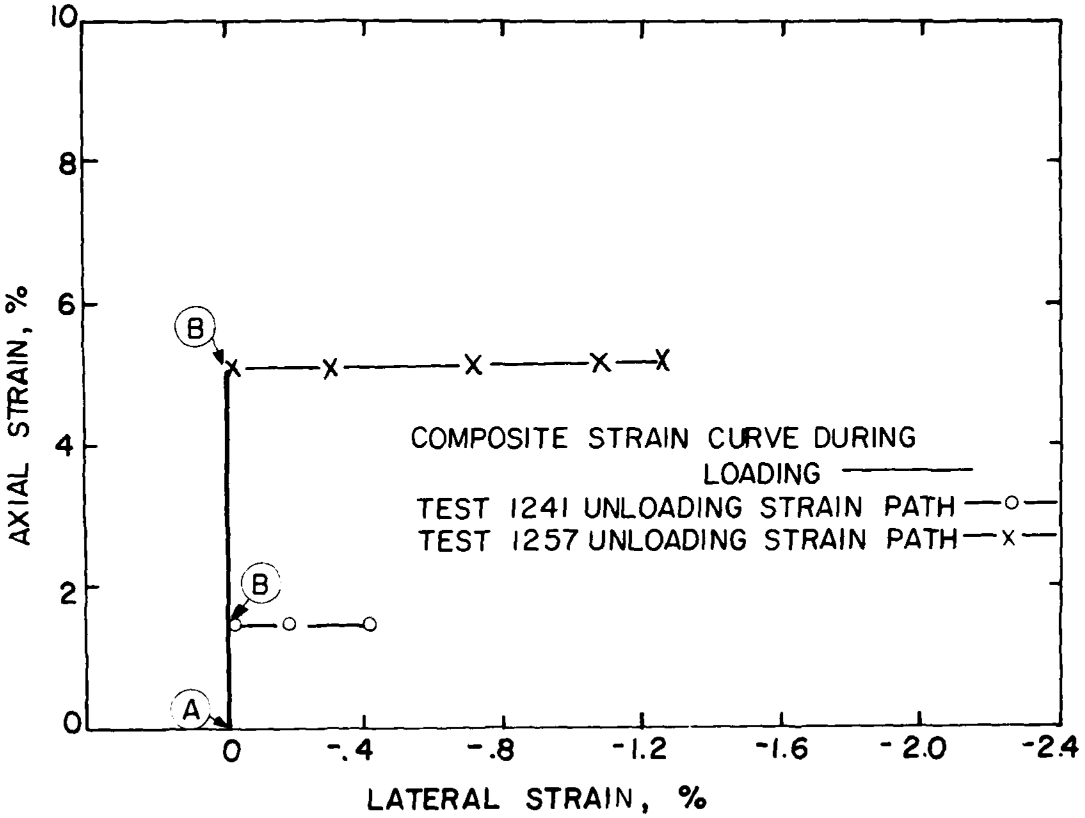

Figure 9d. Strain path followed during path II testing.

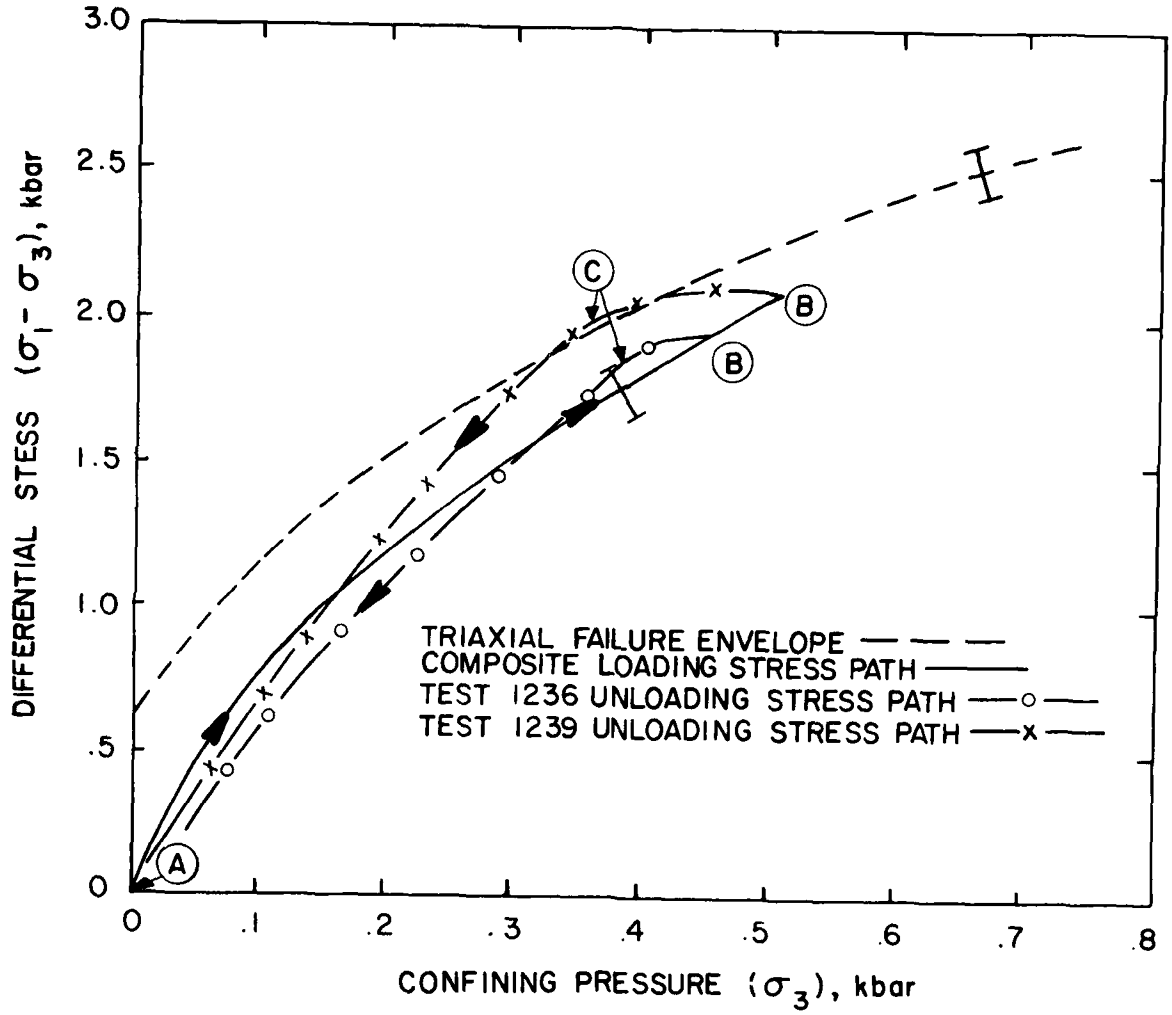

Figure 9e. Stress path followed during strain path I testing.

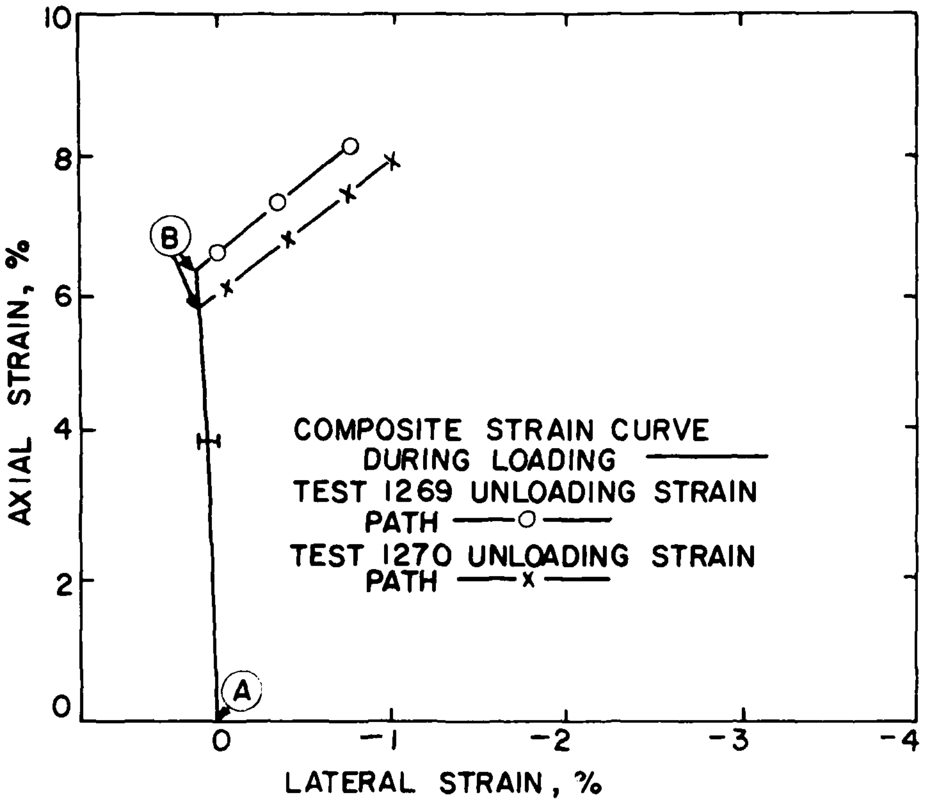

Figure 9f. Strain path followed during path III testing.

DISTRIBUTION LIST

DEPARTMENT OF DEFENSE

Assistant to the Secretary of Defense
Atomic Energy
ATTN: Executive Assistant

Defense Advanced Rsch Proj Agency
ATTN: G. Bulin

Defense Intelligence Agency
ATTN: DB-4N
ATTN: DB-4C, E. O'Farrell

Defense Nuclear Agency
2 cy ATTN: SPSS
4 cy ATTN: TITL

Defense Technical Info Ctr
12 cy ATTN: DD

Field Command
Defense Nuclear Agency
ATTN: FCPR
ATTN: FCTMOF

Field Command
Defense Nuclear Agency
Livermore Branch
ATTN: FCPRL

Interservice Nuclear Weapons School
ATTN: TTV

Joint Strat Tgt Planning Staff
ATTN: JLA
ATTN: NRI-STINFO Library

NATO School (SHAPE)
ATTN: U.S. Documents Officer

Undersecretary of Defense for Rsch & Engrg
ATTN: Strategic & Space Systems (OS)

DEPARTMENT OF THE ARMY

BMD Advanced Technology Center
Department of the Army
ATTN: ATC-T
ATTN: ICRDABH-X

Chief of Engineers
Department of the Army
ATTN: DAEN-RDL
ATTN: DAEN-MCE-D

Harry Diamond Laboratories
Department of the Army
ATTN: DELHD-N-P
ATTN: DELHD-I-TL

U.S. Army Ballistic Research Labs
ATTN: DRDAR-TSB-S
ATTN: DRDAR-BLV
ATTN: DADAR-BLT, J. Keefer

DEPARTMENT OF THE ARMY (Continued)

U.S. Army Concepts Analysis Agency
ATTN: CSSA-ADL

U.S. Army Engineer Center
ATTN: DT-LRC

U.S. Army Engineer Div Huntsville
ATTN: HNDED-SR

U.S. Army Engineer Div Ohio River
ATTN: ORDAS-L

U.S. Army Engr Waterways Exper Station
ATTN: J. Drake
ATTN: Library
ATTN: WESSA, W. Flathau
ATTN: WESSE, L. Ingram
ATTN: J. Strange
ATTN: J. Zelasko
2 cy ATTN: WESSD, J. Jackson

U.S. Army Material & Mechanics Rsch Ctr
ATTN: Technical Library

U.S. Army Materiel Dev & Readiness Cmd
ATTN: DRXAM-TL

U.S. Army Missile Command
ATTN: RSIC

U.S. Army Nuclear & Chemical Agency
ATTN: Library

DEPARTMENT OF THE NAVY

Naval Civil Engineering Laboratory
ATTN: Code L08A

Naval Electronic Systems Command
ATTN: PME 117-21

Naval Facilities Engineering Cmd
ATTN: Code 04B

Naval Material Command
ATTN: MAT 08T-22

Naval Postgraduate School
ATTN: G. Lindsay
ATTN: Code 1424 Library

Naval Research Laboratory
ATTN: Code 2627

Naval Surface Weapons Center
ATTN: Code F31

Naval Surface Weapons Center
ATTN: Tech Library & Info Svcs Br

Naval War College
ATTN: Code E-11

DEPARTMENT OF THE NAVY (Continued)

Naval Weapons Evaluation Facility
ATTN: Code 10

Naval Underwater Systems Center
ATTN: Code EM, J. Kalinowski

Office of Naval Research
ATTN: Code 474, N. Perrone

Office of Chief of Naval Operations
ATTN: OP 981
ATTN: OP 03EG

Strategic Systems Project Office
Department of the Navy
ATTN: NSP-43

DEPARTMENT OF THE AIR FORCE

Air Force Geophysics Laboratory
ATTN: LWW, K. Thompson

Air Force Institute of Technology
ATTN: Library

Air Force Office of Scientific Rsch
ATTN: W. Best
ATTN: J. Allen

Air Force Systems Command
ATTN: DLW

Air Force Weapons Laboratory
Air Force Systems Command
ATTN: NTES-C, R. Henny
ATTN: NTES, J. Thomas
ATTN: NTE, M. Plamonodon
ATTN: SUL
ATTN: NTES, R. Jolley

Air University Library
Department of the Air Force
ATTN: AUL-LSE

Assistant Chief of Staff
Intelligence
Department of the Air Force
ATTN: INT

Ballistic Missile Office
Air Force Systems Command
ATTN: MNN
ATTN: MNNXH, D. Gage
ATTN: MNNXH, M. Delvecchio

Research, Development, & Acq
Department of the Air Force
ATTN: AFRDQI

Logistics & Engineering
Department of the Air Force
ATTN: LEEE

Foreign Technology Division
Air Force Systems Command
ATTN: NIIS Library

DEPARTMENT OF THE AIR FORCE (Continued)

Rome Air Development Center
Air Force Systems Command
ATTN: TSLD

Strategic Air Command
Department of the Air Force
ATTN: INT J. McKinney
ATTN: NRI-STINFO Library

Vela Seismological Center
ATTN: G. Ullrich

DEPARTMENT OF ENERGY

Department of Energy
Albuquerque Operations Office
ATTN: CTID

Department of Energy
Nevada Operations Office
ATTN: Mail & Recds for Tech Lib

OTHER GOVERNMENT AGENCIES

Central Intelligence Agency
ATTN: OSWR/NED

Department of the Interior
Bureau of Mines
ATTN: Tech Lib

Federal Emergency Management Agency
ATTN: Assistant Associate Dir

DEPARTMENT OF ENERGY CONTRACTORS

Lawrence Livermore National Laboratory
ATTN: Tech Info Dept Lib
ATTN: D. Glenn

Los Alamos National Scientific Laboratory
ATTN: MS 670, J. Hopkins
ATTN: R. Bridwell
ATTN: MS 364

Oak Ridge National Laboratory
Nuclear Division
ATTN: Central Rsch Lib
ATTN: Civil Def Res Proj

Sandia National Laboratories
Livermore Laboratory
ATTN: Lib & Sec Class Div

Sandia National Laboratories
ATTN: L. Hill
ATTN: A. Chabai
ATTN: 3141

DEPARTMENT OF DEFENSE CONTRACTORS

Aerospace Corp
ATTN: Technical Info Svcs

Agbabian Associates
ATTN: M. Agbabian

DEPARTMENT OF DEFENSE CONTRACTORS (Continued)

Applied Research Associates, Inc.
ATTN: H. Auld
ATTN: N. Higgins
ATTN: J. Bratton

Applied Research Associates, Inc
ATTN: S. Blouin

Applied Theory, Inc
2 cy ATTN: J. Trulio

AVCO Research & Systems Group
ATTN: Library A830

BDM Corp
ATTN: Corporate Library
ATTN: T. Neighbors

Boeing Co
ATTN: Aerospace Library

California Institute of Technology
ATTN: T. Ahrens

California Research & Technology, Inc
ATTN: K. Kreyenhagen
ATTN: Library
ATTN: M. Rosenblatt
ATTN: S. Schuster

California Research & Technology, Inc
ATTN: D. Orphal

Calspan Corp
ATTN: Library

University of Denver
ATTN: J. Wisotski

EG&G Washington Analytical Svcs Ctr, Inc
ATTN: Library

Eric H. Wang
Civil Engineering Rsch Fac
University of New Mexico
ATTN: N. Baum

Gard, Inc
ATTN: G. Neidhardt

Horizons Technology, Inc
ATTN: R. Kruger

IIT Research Institute
ATTN: Documents Library
ATTN: R. Welch
ATTN: M. Johnson

Institute for Defense Analyses
ATTN: Classified Library

J.H. Wiggins Co., Inc
ATTN: J. Collins

Kaman AviDyne
ATTN: N. Hobbs
ATTN: Library

Kaman Sciences Corp
ATTN: Library

Kaman Tempo
ATTN: DASIAC

Lockheed Missiles & Space Co., Inc
ATTN: T. Geers
ATTN: Technical Info Ctr

Lockheed Missiles & Space Co., Inc
ATTN: J. Weisner

Lovelace Biomed & Enviro Rch Inst, Inc
ATTN: R. Jones

Martin Marietta Corp
ATTN: G. Freyer

McDonnell Douglas Corp
ATTN: R. Halprin

Merritt CASES, Inc
ATTN: J. Merritt
ATTN: Library

Pacific-Sierra Research Corp
ATTN: H. Brode

Patel Enterprises, Inc
ATTN: M. Patel

Physics International Co
ATTN: L. Behrmann
ATTN: F. Sauer
ATTN: E. Moore
ATTN: Technical Library
ATTN: J. Thomsen

R & D Associates
ATTN: Technical Info Ctr
ATTN: J. Lewis
ATTN: J. Carpenter
ATTN: W. Wright
ATTN: R. Port
ATTN: P. Haas

Science Applications, Inc
ATTN: Technical Library

Science Applications, Inc
ATTN: D. Bernstein
ATTN: D. Maxwell

Science Applications, Inc
ATTN: W. Layson

Southwest Research Institute
ATTN: W. Baker
ATTN: A. Wenzel

DEPARTMENT OF DEFENSE CONTRACTORS (Continued)

SRI International
ATTN: D. Keough
ATTN: G. Abrahamson
ATTN: B. Gasten
ATTN: Y. Gupta

Systems, Science & Software, Inc
ATTN: T. Cherry
ATTN: T. Riney
ATTN: Library
ATTN: D. Grine

Systems, Science & Software, Inc
ATTN: J. Murphy

Terra Tek, Inc
ATTN: S. Green
ATTN: A. Abou-Sayed
ATTN: Library
4 cy ATTN: J. Johnson
4 cy ATTN: D. Schmitz
4 cy ATTN: R. Dropek

DEPARTMENT OF DEFENSE CONTRACTORS (Continued)

Tetra Tech, Inc
ATTN: L. Hwang

TRW Defense & Space Sys Group
ATTN: Technical Info Ctr
ATTN: P. Bhutta
2 cy ATTN: N. Lipner

TRW Defense & Space Sys Group
ATTN: P. Dai
ATTN: E. Wong

Universal Analytics, Inc
ATTN: E. Field

Weidlinger Assoc., Consulting Engineers
ATTN: M. Baron

Weidlinger Assoc., Consulting Engineers
ATTN: J. Isenberg

DATE
ILMED
-8